208

NASA TECHNICAL NOTE

NASA TN D-2503

NASA TN D-2503

EFFECTS OF PURITY AND STRUCTURE ON RECRYSTALLIZATION, GRAIN GROWTH, DUCTILITY, TENSILE, AND CREEP PROPERTIES OF ARC-MELTED TUNGSTEN

by William D. Klopp and Peter L. Raffo

Lewis Research Center
Cleveland, Ohio

NATIONAL AERONAUTICS AND SPACE ADMINISTRATION • WASHINGTON, D. C. • NOVEMBER 1964

EFFECTS OF PURITY AND STRUCTURE ON RECRYSTALLIZATION, GRAIN GROWTH, DUCTILITY, TENSILE, AND CREEP PROPERTIES OF ARC-MELTED TUNGSTEN

By William D. Klopp and Peter L. Raffo

Lewis Research Center
Cleveland, Ohio

NATIONAL AERONAUTICS AND SPACE ADMINISTRATION

For sale by the Office of Technical Services, Department of Commerce,
Washington, D.C. 20230 -- Price $1.25

EFFECTS OF PURITY AND STRUCTURE ON RECRYSTALLIZATION, GRAIN GROWTH, DUCTILITY, TENSILE, AND CREEP PROPERTIES OF ARC-MELTED TUNGSTEN

by William D. Klopp and Peter L. Raffo

Lewis Research Center

SUMMARY

The properties of five lots of arc-melted tungsten have been characterized by chemical analyses, recrystallization and grain growth behavior, low-temperature ductility, and high-temperature tensile and creep studies. Purity appears to affect the recrystallization and grain growth rates, while structure exerts the predominant influence on high-temperature tensile and creep properties.

The recrystallization and grain growth rates varied among the five lots studied, with the purest lots exhibiting higher overall rates than the less pure lots.

The low-temperature tensile ductilities of stress-relieved materials showed the usual decrease in ductile-brittle transition temperature with increasing amounts of prior work. Limited tensile and bend data on recrystallized materials showed no discernible effect of purity, structure, or annealing temperature on the ductile-brittle transition temperature.

The tensile properties of arc-melted tungsten at 2500° to 4140° F were significantly affected by structure, the fine-grained materials being stronger than coarse-grained materials. At constant strain rate, the yield strength varied as the -0.25 power of the average grain diameter and the ultimate tensile strength varied as the -0.12 power of the average grain diameter. Thus, decreasing the average grain diameter from 0.1 to 0.005 centimeter increased the yield strength by 80 percent and the ultimate strength by 40 percent. The parabolic strain-hardening coefficients for recrystallized materials also increase with decreasing grain size.

The creep behavior of arc-melted tungsten at 3000° to 4000° F also was affected by grain size, the fine-grained materials being stronger. At constant stress the creep rate varied as the 0.43 power of the average grain diameter.

INTRODUCTION

As a potential high-temperature structural material, tungsten has for several years been of interest to NASA. This report describes the results of studies on unalloyed arc-melted tungsten conducted at the Lewis Research Center as a portion of a larger study on both unalloyed and alloyed tungsten.

The properties of powder-metallurgy tungsten, which has been a commercial product for several decades, have been well documented in the literature; however, less information is available on tungsten consolidated by melting processes. Several recent studies have generated information on recrystallization (ref. 1), low-temperature ductility (ref. 1), and high-temperature tensile strength (refs. 2 and 3) of arc-melted tungsten. Studies have also been conducted on the recrystallization (refs. 4 to 6) and low-temperature ductility (refs. 7 and 8) of single-crystal tungsten and on the properties of polycrystalline electron-beam-melted tungsten (refs. 4, 9, and 10). None of these studies, however, covered the creep properties of melted tungsten. Additionally, the effects of purity and structure on recrystallization, grain growth, and mechanical properties have not been well defined.

The present study was conducted in order to provide more detailed information on purity and structural effects on the recrystallization, grain growth, low-temperature ductility, and high-temperature tensile and creep behavior of arc-melted tungsten. This information should provide baseline data for the development of arc-melted tungsten-base alloys and for comparison with powder-metallurgy and electron-beam-melted tungsten materials.

SYMBOLS

A, A', B, c, k	constant
a	exponential stress dependency
b	exponential grain size factor
C	circumference of circle, 48.3 cm
e	engineering strain
$\dot{e}$	steady creep rate, sec^{-1}
f	grain shape factor
G	boundary migration rate, cm/sec
K	parabolic grain growth rate, sq cm/sec
L	average grain diameter, cm
L_o	initial average grain diameter, cm
M	magnification

m	rupture time-creep rate exponent
$\bar{N}$	average number of grains per unit volume, cm^{-3}
$\bar{N}_o$	average number of recrystallization nuclei per unit volume, cm^{-3}
n	number of intercepts
Q	activation energy for creep, cal/g-mole
Q_R	activation energy for grain boundary migration, cal/g-mole
R	gas constant, 1.987 cal/g-mole
S	engineering stress, psi
T	temperature, ^oK
t	time, sec
t_r	rupture time, sec
UTS	ultimate tensile strength, psi
X	fraction recrystallized
YS	yield strength, psi
β	transient creep rate, $sec^{-1/3}$
ϵ	true plastic strain
σ	true stress, psi
χ	strain hardening coefficient, psi^2

EXPERIMENTAL PROCEDURES

Starting Materials

The starting materials consisted of sintered unalloyed (undoped) 15-pound tungsten electrodes. Five electrodes on which the majority of the studies were conducted are identified as A to E. These are ranked according to the analyses of the subsequent fabricated materials, with A containing the least impurities and E containing the most impurities. The electrodes measured $1\frac{1}{8}$ inches in diameter by 24 inches long (electrodes A, B, D, and E) or 15/16 inch in diameter by 35 inches long (electrode C) and were approximately 85 percent dense. Two additional lots, designated F and G, were employed in limited creep studies. These were prepared and processed similarly to lots A to E.

Melting

The five 15-pound electrodes were consumably arc-melted in vacuum into an 18-inch deep, 2.68-inch-diameter water-cooled copper mold by using direct current, straight polarity (electrode negative) power. Melting currents were 4200 to 4400 amperes at 35 volts, giving average melt rates of 2.20 to 2.77 pounds per minute. The furnace was equipped with two 36-inch-diameter oil-diffusion pumps and was evacuated to a chamber pressure of approximately 0.01 micron during melting. Actual pressures at the molten ingot tops were undoubtedly much higher, as has been shown with molybdenum (ref. 11).

Primary Fabrication

Initial ingot breakdown was accomplished by hot extrusion, since the large grained ingots are not amenable to other types of fabrication directly. Ingot A was machined to 1.75 inches in diameter by 4 inches long and impact extruded, as indicated in table I. Ingots B to E were machined to 2.08 inches in

TABLE I. - EXTRUSION DATA FOR ARC-MELTED TUNGSTEN

	Billet identity				
	A	B	C	D	E
Extrusion press	(a)	(b)	(b)	(b)	(b)
Preheat temperature, ^{o}F	3425	3450	3400	3460	3450
Reduction ratio	10	6	8	6	6
Extrusion speed, in./min	---	---	5.4	5.8	5.7
Extrusion constant, K, psi[c]	---	92.4×10^{3}	68.5×10^{3}	98.4×10^{3}	88.4×10^{3}
Hardness of extruded rod, VHN[d]	383	385	458	453	376
Fraction not recrystallized	0	0	0.6	1.0	0
Average grain diameter, L, cm	4.1×10^{-3}	4.0×10^{-3}	---	---	3.8×10^{-3}

[a]Impact extrusion press.

[b]Hydropress.

[c]Extrusion constant, $K = P/\ln R$, where P is maximum pressure on billet in psi and R is reduction ratio.

[d]10-kg load.

diameter by $3\frac{1}{2}$ to 4 inches long and extruded at slower speeds in a 1000-ton hydropress. Extrusion constants varied from 68,500 psi for billet C to 98,400 psi for billet D, as shown in table I. All five billets were completely extruded and suffered very little surface tearing.

Secondary Fabrication

After sectioning to obtain metallographic samples, portions of each extrusion were warm swaged to 0.36 inch in diameter to provide material for tensile specimens or to various sizes as small as 0.18 inch in diameter to provide material for recrystallization and grain growth studies. Additionally, portions of extrusions B and D were warm fabricated by straight and cross rolling

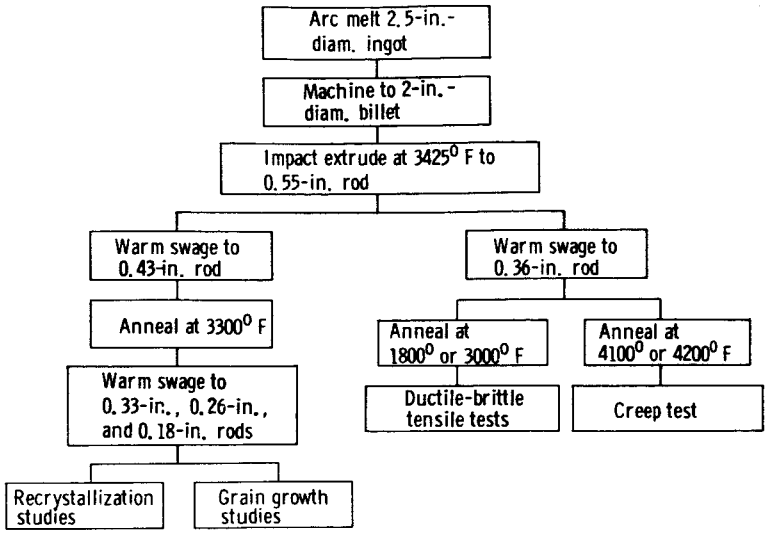

(a) Lot A.

Figure 1. - Fabrication and evaluation flow diagrams.

to 0.03- to 0.05-inch-thick sheet, as indicated in the flow sheets for lots A to E shown in figure 1. All swaging and rolling was initiated at 2500° F and completed at 2100° F, with the exception of material swaged from lot A for recrystallization studies. This material was swaged entirely at 2150° F to maximize cold working.

Chemical Analyses

Average chemical analyses of machined specimens of the 0.36-inch-diameter rod swaged from each of the five extrusions are given in table II. Original analyses of these fabricated rods and of four starting electrodes are given in the appendix. These analyses show that all five lots contained between 15 and 23 parts per million total interstitials, with the major variation being the threefold difference in oxygen content between lots B and C. In contrast, the total detectable metallic impurity contents varied from 25 to 88 parts per million, with lot E containing approximately 10 times as much aluminum and iron as lot A. The amounts of copper, nickel, and silicon, although lower than those of aluminum and iron, were also highest in lot E.

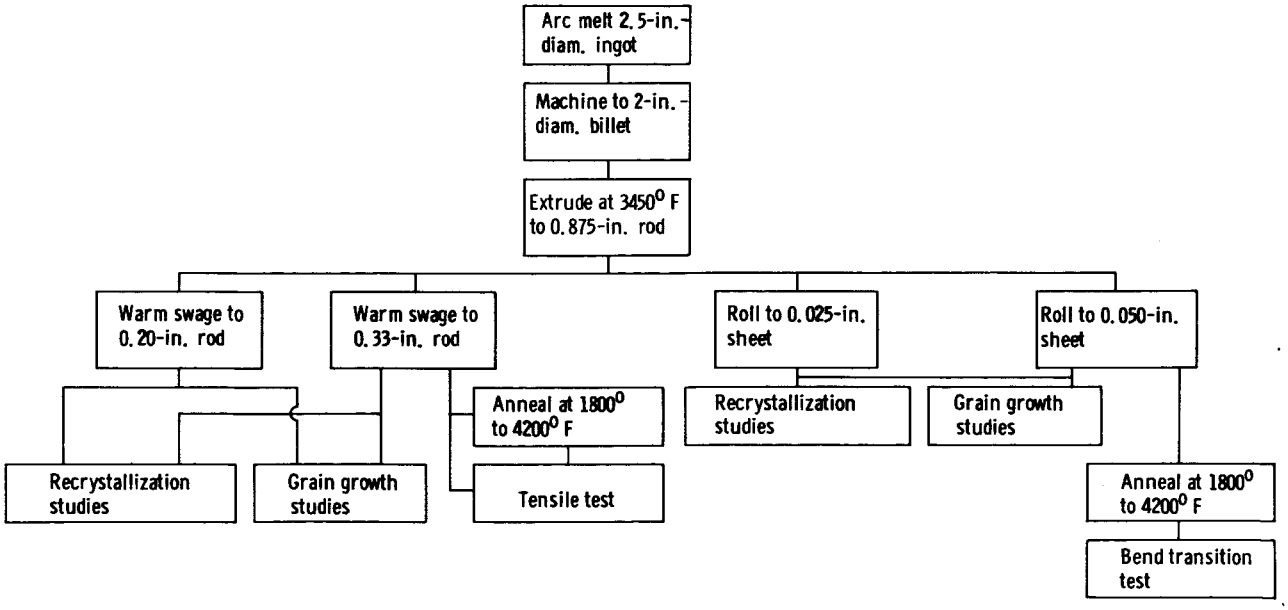

(b) Lot B.

Figure 1. - Continued. Fabrication and evaluation flow diagrams.

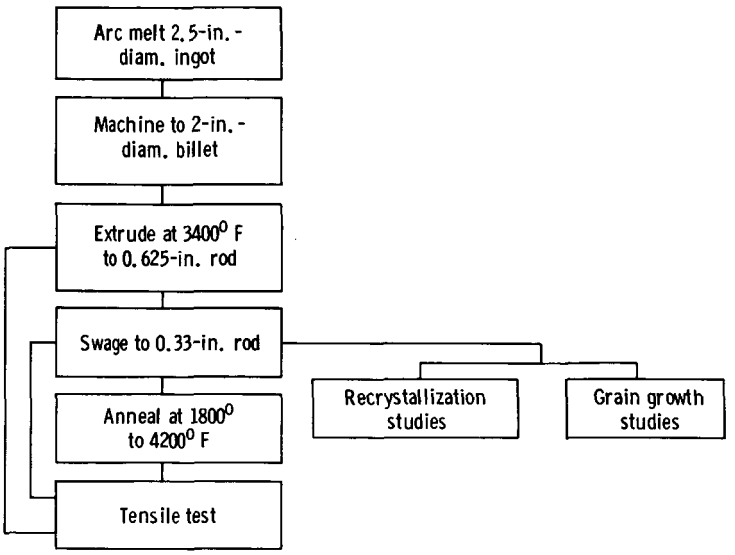

(c) Lot C.

Figure 1. - Continued. Fabrication and evaluation flow diagrams.

It is believed that these very small purity differences reflect both starting material purity and consolidation procedures and, further, that they affect the recrystallization and grain growth characteristics of the various lots, as described in the sections Recrystallization Behavior and Grain Growth Behavior.

Recrystallization and Grain Growth Studies

Recrystallization studies were conducted on rod and/or sheet from each of the five lots under study. Rod samples approximately 3/8 inch long and sheet samples about 1/4 inch wide by 3/8 inch long were annealed for times ranging from 8 minutes to 20 hours at temperatures ranging from 2550° to 3000° F. Annealing treatments of 4-hours duration or less were conducted in an induction-heated hydrogen-atmosphere furnace, while the longer treatments at 2550° F were conducted in a resistance-heated vacuum furnace. Temperatures were measured with a tungsten - tungsten-26 percent rhenium thermocouple (hydrogen furnace) or a platinum - platinum-10 percent rhodium thermocouple (vacuum furnace) and are estimated accurate to ±15° F.

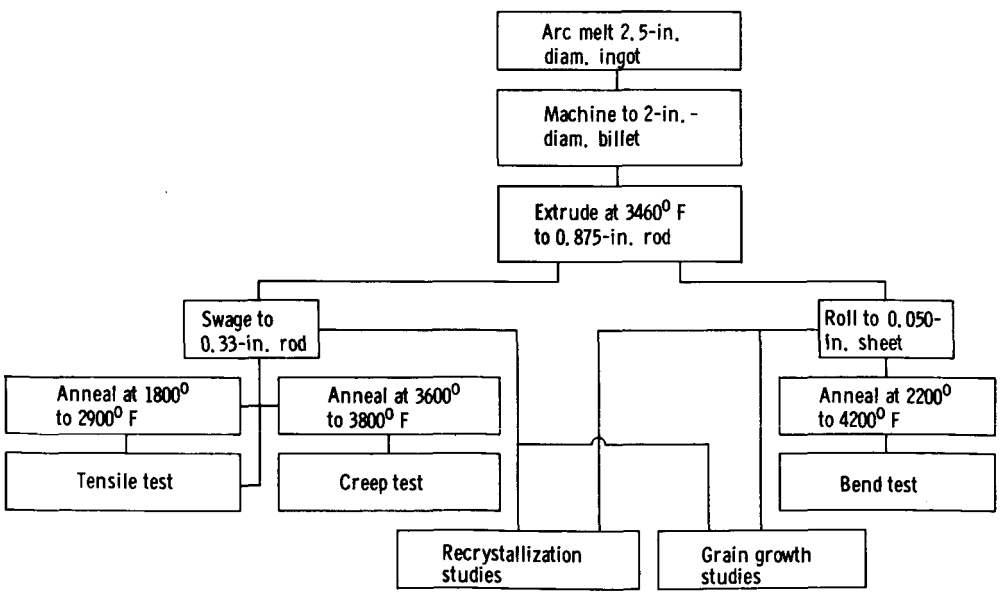

(d) Lot D.

Figure 1. - Continued. Fabrication and evaluation flow diagrams.

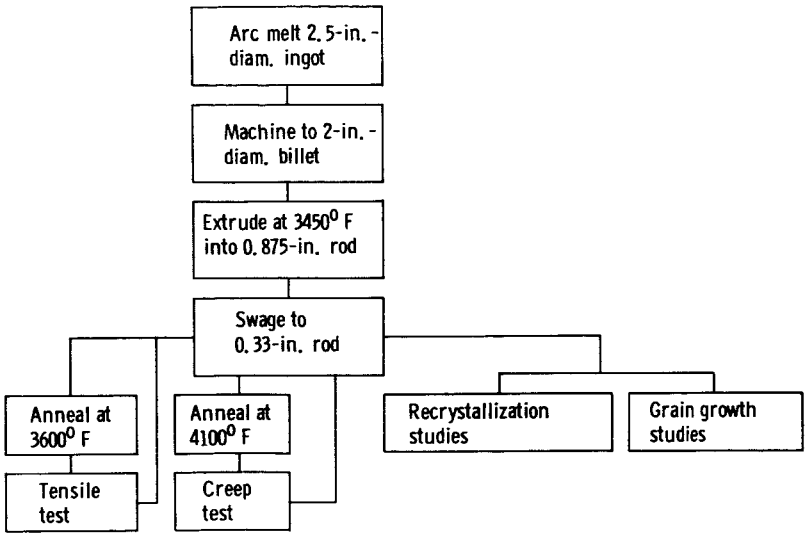

(e) Lot E.

Figure 1. - Concluded. Fabrication and evaluation flow diagrams.

TABLE II. - ANALYSES OF FABRICATED ARC-MELTED TUNGSTEN RODS

Element	Lot				
	A	B	C	D	E
	Impurity, ppm[a]				
Oxygen	3.0	2.0	6.0	5.0	3.0
Nitrogen	13.0	9.0	8.0	9.0	12.0
Carbon	6.0	4.0	9.0	6.0	5.0
Hydrogen	<1.0	<1.0	<1.0	<1.0	<1.0
Aluminum	1.5	2.2	8.0	5.0	15.0
Chromium	<3.0	<3.0	<3.0	<3.0	4.0
Copper	1.1	.7	.7	.7	2.6
Iron	4.0	11.0	12.0	16.0	38.0
Molybdenum	10.0	11.0	10.0	12.0	11.0
Nickel	1.2	1.2	1.2	1.1	5.6
Silicon	7.5	8.0	7.5	7.0	12.0
Sodium	<5.0	<5.0	<5.0	16.0	<5.0
Total detectable metallics	25.3	34.1	39.4	57.8	88.2

[a]Analyses conducted as follows:
Oxygen and hydrogen - vacuum fusion
Nitrogen - Kjeldahl
Carbon - combustion
Metallics - average of emission spectrography and mass spectrography. Only elements detected by both emission and mass spectrography are reported. Original analyses are given in appendix.

The heat-treated samples were sectioned longitudinally, mounted, and examined metallographically. The fraction recrystallized was averaged from estimates by two observers over at least 10 areas on each sample. The average grain diameter was determined for specimens recrystallized 90 percent or more by counting the number of boundary intercepts with a circle 48.3 centimeters in circumference on a projection screen. The following relation was employed in calculating the grain diameter:

$$L = \frac{C}{Mn} \qquad (1)$$

where

L average grain diameter, cm

C circumference of circle, 48.3 cm

M magnification

n number of intercepts

At least five counts of about 40 intercepts each were averaged for each specimen. The number of grains per cubic centimeter is calculated (ref. 12) as

$$\overline{N} = \left(\frac{1}{L}\right)^3 \qquad (2)$$

where

$\overline{N}$ average number of grains per cubic centimeter

L average grain diameter, cm

Grain growth studies were also conducted on 3/8-inch-long rod samples and/or 1/4-inch-wide by 3/8-inch-long sheet samples from each of the five lots. These were annealed at temperatures ranging from 3300° to 4200° F (for times ranging from 1 to 14 hr). Annealing treatments were conducted in a tungsten-element vacuum furnace. Temperatures were measured by optical pyrometry and are believed accurate to ±25° F. The initial grain size for worked samples was taken as that which was characteristic of the same material immediately after recrystallization. For preannealed samples, the initial sizes were determined by the intercept-count method previously described. Final grain sizes were determined similarly after annealing.

Bend Transition Studies

Bend specimens, 3/8 by 3/4 inch, were cut from a 0.050-inch-thick sheet rolled from extruded bars of lots B and D. The specimens were electropolished for 10 minutes at 12 volts direct current in a 2-percent sodium hydroxide aqueous solution to produce smooth, scratch-free specimen surfaces. Bend tests were conducted in the apparatus pictured in figure 2. The specimens were mounted between the three rollers and pulled in tension to produce three-point

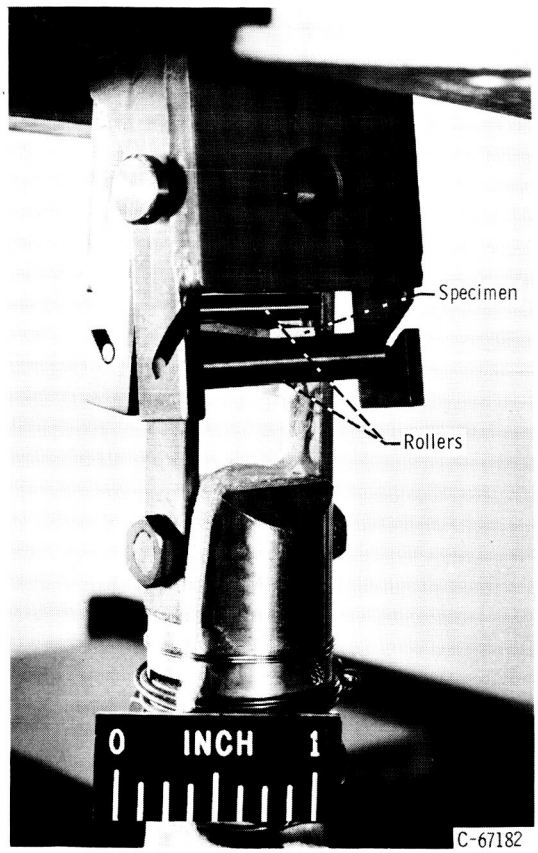

(a) Close-up view showing tungsten sheet specimen held between three rollers.

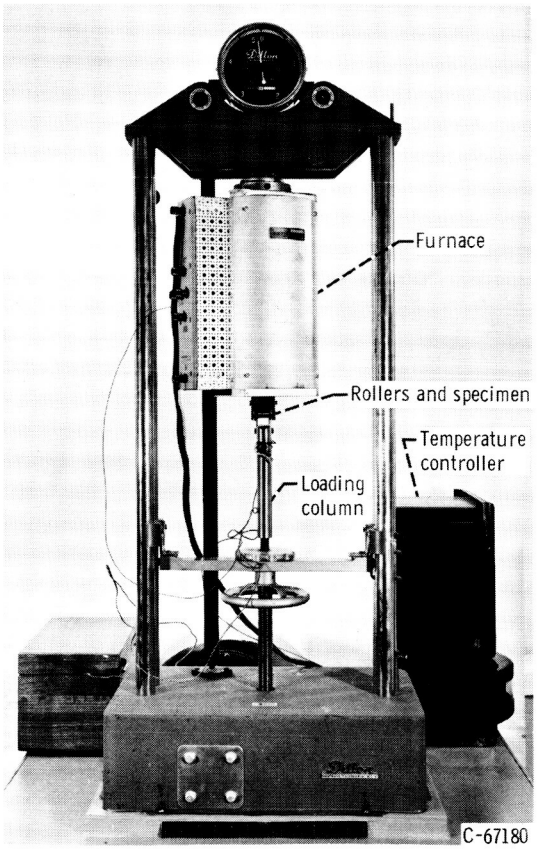

(b) Overall view showing tensile machine, temperature controller, loading column, rollers, specimen, and furnace.

Figure 2. - Apparatus for bend testing tungsten sheet at temperatures from ambient to 1000° F.

bending. Elevated temperatures were obtained with a platinum-wound resistance furnace. All the tests were run in air. Temperature was measured by a Chromel-Alumel thermocouple mounted on the roller assembly 1/16 inch from the specimen. The tests were performed by allowing the specimen to heat slowly to within 5° F of the test temperature, after which the specimen was bent at a roller travel speed of 2 inches per minute until failure. Temperature overshoot was no more than 5° F during the run. All tests were made employing a ratio of bend radius to sheet thickness of 4.

Tensile and Creep Studies

Tensile specimens for both low- and high-temperature tensile tests and high-temperature creep tests were machined from 0.36-inch-diameter swaged rod. The specimens had a reduced section 1.03 inches long and 0.160 inch in diameter.

For low-temperature testing, in order to determine the ductile-brittle transition, the sample surfaces were electropolished in the sodium hydroxide solution described previously. This procedure, which removed 4 to 5 mils of the tungsten from the surface, has been shown (ref. 13) to improve the reproducibility of tensile ductility data and also to lower the ductile-brittle transition temperature moderately by reducing surface roughness. Testing was conducted in vacuum at a crosshead movement rate of 0.005 inch per minute to about 0.5 percent plastic strain in order to define the 0.2 percent offset yield strength, after which the crosshead movement rate was increased to 0.05 inch per minute to fracture.

Tensile tests at 2500° to 4140° F were conducted in an evacuated chamber (1×10^{-5} mm Hg) equipped with a tantalum sleeve heater, which has been described previously (ref. 14). Crosshead movement rates were the same as those employed for low-temperature testing. Specimen extension during testing was taken as equal to the crosshead movement.

Step-load creep tests were conducted in the same tensile unit and vacuum furnace as employed for the high-temperature tensile tests. For these tests, the loads were increased by approximately 10 percent at 15-minute intervals.

Constant-load creep tests were conducted in a conventional beam-load machine equipped with a vacuum shell and tantalum heater similar to that used for tensile testing. Specimen extensions were measured from loading rod movement. These measurements were corrected for settling and extension in the pull rods based on a correlation between optical data on specimen extension and total load train extension.

Grain sizes were measured in the heated but undeformed shoulders of all tensile and creep samples after testing.

RESULTS AND DISCUSSION

Recrystallization Behavior

Recrystallization studies were conducted on rod and/or sheet from each of

TABLE III. - RECRYSTALLIZATION DATA FOR ARC-MELTED TUNGSTEN AT 2550° TO 3000° F

Material geometry	Average just-recrystallized grain diameter,[a] L_o, cm	Average number of grains per cubic centimeter, $\bar{N}$	Reduction in area, percent[b]	Annealing condition		Fraction recrystallized	Hardness (10-kg load), VHN	Average grain diameter, L, cm	Boundary migration rate, G, cm/sec
				Temperature, °F	Time, t, hr				
Lot A									
0.33-in.-diam. rod	2.41×10^{-2}	7.09×10^{4}	[c]40.8	As swaged		-----	425	---------	--------
				2550	1	0.0	433	---------	--------
					4	0.0	429	---------	--------
					7	.50	401	---------	8.5×10^{-7}
					20	.80	375	---------	3.9
					20	.85	381	---------	4.2
				2730	1	0.05	421	---------	2.5×10^{-6}
					2	.35	401	---------	2.5
					4	.60	383	---------	1.6
0.26-in.-diam. rod	1.27×10^{-2}	4.88×10^{5}	[c]63.3	As swaged		-----	455	---------	--------
				2550	1	0.0	450	---------	--------
					4	.30	409	---------	6.3×10^{-7}
					4	.35	405	---------	6.7
					7	.97	370	16.2×10^{-3}	7.7
					20	1.00	366	12.8	--------
				2730	0.5	0.48	387	---------	6.1×10^{-6}
					1	.19	405	---------	2.1
					2	.95	357	10.3×10^{-3}	2.5
0.18-in.-diam. rod	6.23×10^{-3}	4.13×10^{6}	[c]82.6	As swaged		-----	478	---------	--------
				2550	0.13	0.0	437	---------	--------
					1.0	.01	450	---------	3.7×10^{-7}
					2.0	.43	392	---------	7.1
					4.0	.73	373	---------	4.7
				2730	0.25	0.56	367	---------	6.5×10^{-6}
					.50	.74	364	---------	3.8
					1.0	1.00	369	6.23×10^{-3}	--------
Lot B									
0.36-in.-diam. rod	4.86×10^{-3}	8.40×10^{6}	83.0	2600	1.0	0.079	446	---------	5.9×10^{-7}
				2800	1.0	1.00	354	5.77×10^{-3}	--------
				3000	1.0	1.00	370	4.08	--------
0.20-in.-diam. rod	3.44×10^{-3}	2.44×10^{7}	94.8	2600	1.0	0.275	425	---------	6.6×10^{-7}
				2800	1.0	1.00	363	3.75×10^{-3}	--------
				3000	1.0	1.00	376	3.16	--------
0.025-in.-thick sheet	3.42×10^{-3}	2.50×10^{7}	97.2	2600	1.0	0.317	442	---------	6.9×10^{-7}
				3000	1.0	1.00	373	3.42×10^{-3}	--------
Lot C									
0.33-in.-diam. rod	4.96×10^{-3}	8.26×10^{6}	81.0	2600	1.0	0.65	409	---------	1.4×10^{-6}
				2800	1.0	1.00	363	5.05×10^{-3}	--------
				3000	1.0	1.00	373	4.86	--------
Lot D									
0.36-in.-diam. rod	4.61×10^{-3}	1.02×10^{7}	83.0	2600	1.0	0.0	455	---------	--------
				2800	1.0	.09	442	---------	5.8×10^{-7}
				3000	1.0	1.00	376	4.61×10^{-3}	--------
0.05-in.-thick sheet	2.66×10^{-3}	5.29×10^{7}	94.3	2600	1.0	0.0	468	---------	--------
				2800	1.0	.068	478	---------	3.1×10^{-7}
				3000	1.0	1.00	380	2.66×10^{-3}	--------
Lot E									
0.36-in.-diam. rod	4.08×10^{-3}	1.47×10^{7}	83.0	2600	1.0	0.0	455	---------	--------
				2800	1.0	.045	450	---------	5.7×10^{-7}
				3000	1.0	1.00	373	4.38×10^{-3}	--------

[a]The just-recrystallized average grain diameter is averaged from measurements on recrystallization specimens (this table) and on grain growth specimens (table V) where no increase in grain size was measurable. The average number of nucleation sites per cubic centimeter is calculated from the average grain diameter by eq. (2).

[b]Reduction after extrusion except where indicated.

[c]Reduction after annealing for 1 hr at 3300° F.

the five lots under study. The purpose was to determine the variations in behavior among the lots and the effects of variations in prior strain and time and temperature of annealing. Data from these studies are presented in table III.

Typical microstructures of partly and fully recrystallized materials are shown in figure 3. These also illustrate the fairly wide difference in recrystallization behavior exhibited by the various lots.

The effects of varying the amount of prior strain were studied on material from lot A and, to lesser extents, on materials from lots B and D. Increasing the prior strain reduced the time required for recrystallization at a given temperature in lots A and B, while very limited data for lot D showed little effect. This lot, as described earlier, was the only one to exhibit a worked structure after extrusion. Lots A, B, and D also exhibited the usual effect of decreasing recrystallized grain size with increasing prior strain.

In order to compare more quantitatively the recrystallization behavior of the various lots, the data were correlated in terms of a nucleation and growth transformation by the Johnson-Mehl relation (ref. 15)

$$X = 1 - e^{-f\overline{N}_o G^3 t^3} \tag{3}$$

where

X fraction recrystallized

f grain shape factor, 1

$\overline{N}_o$ average number of recrystallization nuclei per unit volume, cm^{-3}

G boundary migration rate, cm/sec

t time, sec

The rate of boundary migration G has been shown (ref. 15) to be essentially independent of prior strain at strains greater than about 0.15 and has the same activation energy as that for grain boundary self-diffusion. It may be taken as an indication of the annealing response of a given material.

In the computation of the boundary migration rate, the number of nucleation sites $\overline{N}_o$ is taken as equal to the number of new grains per cubic centimeter, $\overline{N}$ shown by equation (2), as was also done in reference 16. This is in accord with recent recrystallization theory, as expressed in references 17 and 18. New grains are thought to be formed by coalescence of subgrains (formed during prior straining) through solution of the dislocation arrays making up the low-angle boundaries. As the subgrains become coarse, the disorientation between neighboring subgrains increases and the boundaries become more mobile. The high-angle boundaries formed are then capable of moving by strain-induced

(a) Lot B; temperature, 2600° F; 7.9 percent recrystallized.

(b) Lot E; temperature, 2600° F; 0 percent recrystallized.

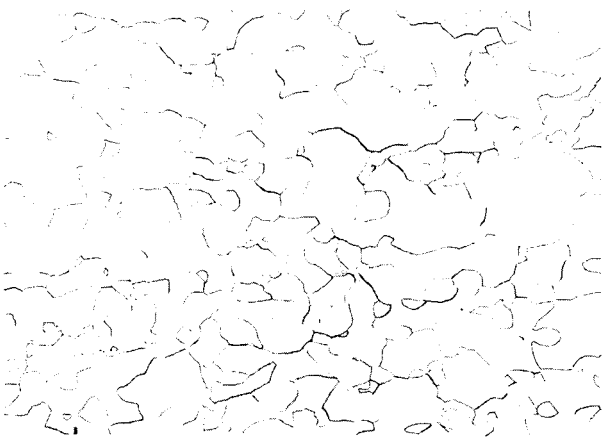

(c) Lot B; temperature, 2800° F; 100 percent recrystallized.

(d) Lot E; temperature, 2800° F; 4.5 percent recrystallized.

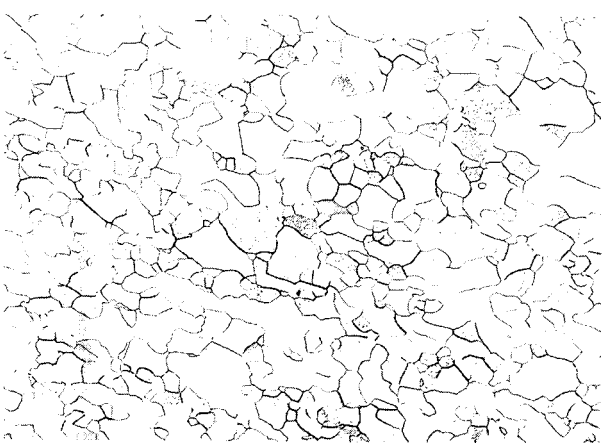

(e) Lot B; temperature, 3000° F; 100 percent recrystallized.

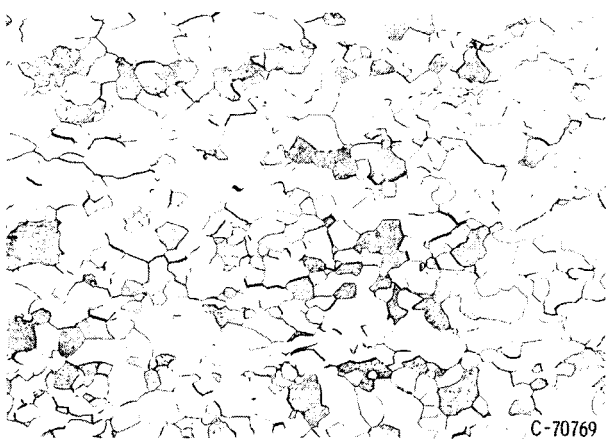

(f) Lot E; temperature, 3000° F; 100 percent recrystallized.

Figure 3. - Microstructures of specimens from lots B and E after swaging 83 percent and annealing for 1 hour at various temperatures. X100. (Reduced 20 percent in printing.)

boundary migration until the new recrystallized grains impinge on one another.)

Values for the number of recrystallization nuclei $\bar{N}_O$ and the calculated boundary migration rate G are included in table III. It is seen that the boundary migration rates are independent of the degree of prior strain (within the limits of experimental error) for a given lot of material. Thus, the recrystallization behavior of each lot may be semiquantitatively described in terms of the number of recrystallization nuclei $\bar{N}_O$, which is a function of prior strain, and the rate of strain-induced boundary migration G, which varies with temperature.

The average boundary migration rates for the various lots are given in table IV and plotted in figure 4. The temperature dependency of G may be expressed by

$$G = G_O e^{-Q_R/RT} \qquad (4)$$

from which the activation energy Q_R for boundary migration in lot A is calculated as 104,500 calories per gram-mole. This value is close to the activation energy of about 100,000 calories per gram-mole obtained in reference 19 for recrystallization of undoped powder-metallurgy tungsten rod. These activation energy values are also close to those for grain boundary self-diffusion, which has been estimated as 0.4 to 0.7 of the volume self-diffusion activation energy (refs. 20 and 21). Taking the latter term as 153,000 calories per gram-mole (ref. 22) gives the estimated range as 61,000 to 107,000 calories per gram-mole. That the observed values lie toward the high end of this estimated range may be taken as an indication of impurity segregation to the grain boundaries (refs. 20 and 23).

TABLE IV. - AVERAGE RECRYSTALLIZATION RATES FOR ARC-MELTED TUNGSTEN AT 2550° TO 2800° F

Lot	Temperature, °F	Reduction in area, percent	Logarithmic average of boundary migration rate for each reduction, cm/sec	Logarithmic average of boundary migration rate for each lot, cm/sec
A	2550	40.8 63.3 82.6	5.2×10^{-7} 6.9 5.0	5.6×10^{-7}
	2730	40.8 63.3 82.6	2.2×10^{-6} 3.2 5.0	3.3×10^{-6}
B	2600	83.0 94.8 97.2	5.9×10^{-7} 6.6 6.9	6.5×10^{-7}
C	2600	81.0	1.4×10^{-6}	1.4×10^{-6}
D	2800	83.0 94.3	5.8×10^{-7} 3.1	4.4×10^{-7}
E	2800	83.0	5.7×10^{-7}	5.7×10^{-7}

In comparing the calculated boundary migration rates with the analytical data in table I, it appears that the three purest lots, A, B, and C, have migration rates that are appreciably greater than those for the less pure lots, D and E. This qualitative relation between purity and recrystallization behavior is in accord with recent studies indicating that dilute alloy additions are extremely effective in reducing the rates of strain-induced boundary migration (refs. 23 and 24).

It should also be recognized that impurities can affect the rate of

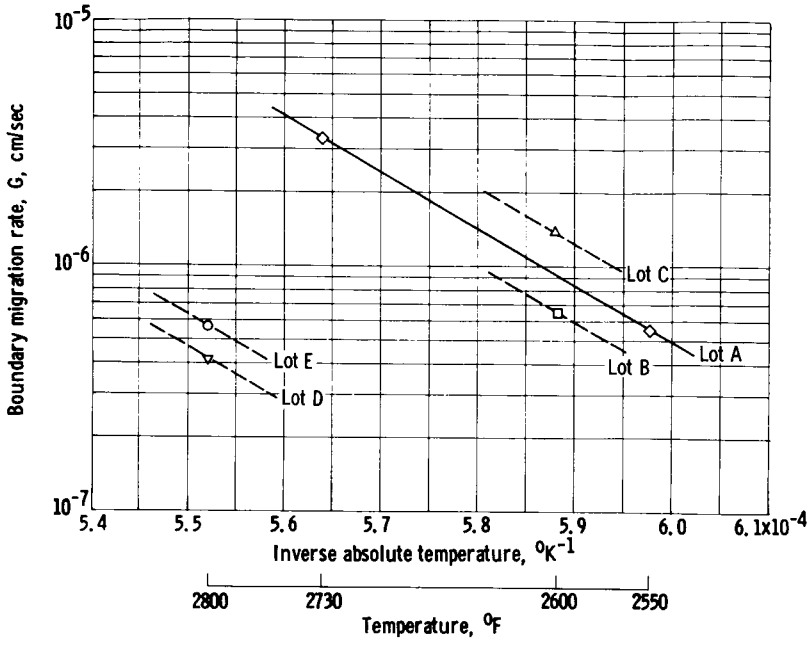

Figure 4. - Temperature dependence of strain-induced boundary migration rates of arc-melted tungsten.

subgrain coalescence prior to the formation of small, high-boundary-angle nuclei, as shown by the results of reference 25. A reduction in the rate of subgrain coalescence would reduce the apparent rate of nucleation without reducing the total number of nuclei and would show up in the correlation employed here as an apparent reduction in the strain-induced boundary migration rate G. Thus, it is not yet clear whether the major effect of impurities is in reduction of low-angle subgrain growth or in the subsequent high-angle boundary migration rate. It does appear, however, that certain impurities, which most likely include aluminum, chromium, iron, nickel, and silicon, decrease the rate of the overall recrystallization process in arc-melted tungsten.

Grain Growth Behavior

Grain growth behavior of each of the five lots were studied by annealing swaged or rolled material for times from 1 to 14 hours at 3300° to 4200° F. The average grain diameters before and after the various annealing treatments are summarized in table V.

In order to compare the grain growth characteristics of the individual lots quantitatively, it was assumed that grain growth was ideal; that is, the migration of the individual boundaries was not retarded by precipitates or microvoids. The equation relating grain size and time at a given temperature under these ideal conditions has been given in reference 26 as

$$L^2 - L_o^2 = Kt \tag{5}$$

where

L final average grain diameter, cm

L_o initial average grain diameter, cm

K parabolic growth rate, sq cm/sec

t time, sec

TABLE V. - GRAIN GROWTH DATA FOR ARC-MELTED TUNGSTEN AT 3300° TO 4200° F

Material geometry	Estimated initial grain diameter, L_o, cm	Reduction in area by swaging, percent	Annealing condition		Final grain diameter, L, cm	Rate constant, K, cm^2/sec
			Temperature, °F	Time, t, hr		
Lot A						
0.33-in.-diam. rod	2.18×10^{-2}	40.8	3500	1	2.79×10^{-2}	--------
			3800	1	2.20	--------
			4000	1	2.30	--------
			4200	2	3.09	6.7×10^{-8}
0.26-in.-diam. rod	1.25×10^{-2}	63.3	3500	1	1.07×10^{-2}	--------
			3800	1	1.43	--------
			4000	1	1.29	--------
			4200	2	2.86	9.2×10^{-8}
0.78-in.-diam. rod	7.05×10^{-3}	82.6	3500	1	7.9×10^{-3}	3.5×10^{-9}
				5	1.17×10^{-2}	4.9
				14	1.57×10^{-2}	3.9
			3800	1	9.9×10^{-3}	1.3×10^{-8}
				2	1.8×10^{-2}	3.8
				4	1.92×10^{-2}	2.2
			4000	1	1.18×10^{-2}	2.2×10^{-8}
				2	2.73	9.7
			4200	2	4.0×10^{-2}	2.2×10^{-7}
Lot B						
0.36-in.-diam. rod	4.86×10^{-3}	----	3500	1	9.19×10^{-3}	1.7×10^{-8}
			3800	1	2.30×10^{-2}	1.4×10^{-7}
			4000	1	5.61×10^{-2}	8.7×10^{-7}
			4200	1	9.54×10^{-2}	2.5×10^{-6}
0.20-in.-diam. rod	3.44×10^{-3}	----	3300	1	5.09×10^{-3}	4.2×10^{-9}
			3500	1	7.31×10^{-3}	1.2×10^{-8}
			3800	1	2.22×10^{-2}	1.3×10^{-7}
Lot C						
0.36-in.-diam. rod	4.96×10^{-3}	----	3500	1	7.52×10^{-3}	8.9×10^{-9}
			3800	1	1.78×10^{-2}	8.1×10^{-8}
			4000	1	5.56×10^{-2}	8.5×10^{-7}
			4200	1	1.04×10^{-1}	3.0×10^{-6}
Lot D						
0.36-in.-diam. rod	4.52×10^{-3}	----	3500	1	5.43×10^{-3}	2.5×10^{-9}
			3800	1	6.27×10^{-3}	5.0×10^{-9}
			4000	1	1.53×10^{-2}	5.9×10^{-8}
			4200	1	6.68×10^{-2}	1.2×10^{-6}
0.05-in.-thick sheet	2.66×10^{-3}	----	3300	1	3.03×10^{-3}	5.8×10^{-10}
			3500	1	4.04×10^{-3}	2.5×10^{-9}
			3800	1	2.42×10^{-2}	1.6×10^{-8}
Lot E						
0.36-in.-diam. rod	4.08×10^{-3}	----	3500	1	4.65×10^{-3}	1.4×10^{-9}
			4000	1	9.88×10^{-3}	2.3×10^{-8}
			4200	1	2.52×10^{-2}	1.7×10^{-7}

TABLE VI. - AVERAGE GRAIN GROWTH RATES FOR ARC-MELTED TUNGSTEN AT 3300° TO 4200° F

Temperature, °F	Logarithmic average of grain growth rate at each temperature, cm^2/sec
Lot A	
3500	4.1×10^{-9}
3800	2.2×10^{-8}
4000	4.6×10^{-8}
4200	2.2×10^{-7}
Lot B	
3300	3.2×10^{-9}
3500	1.4×10^{-8}
3800	1.4×10^{-7}
4000	8.7×10^{-7}
4200	2.5×10^{-6}
Lot C	
3500	8.9×10^{-9}
3800	8.1×10^{-8}
4000	8.5×10^{-7}
4200	3.0×10^{-6}
Lot D	
3300	5.8×10^{-10}
3500	2.5×10^{-9}
3800	1.1×10^{-8}
4000	5.9×10^{-8}
4200	1.2×10^{-6}
Lot E	
3500	1.4×10^{-9}
4000	2.3×10^{-8}
4200	1.7×10^{-7}

This equation was used to calculate a value of K for each annealing treatment by assuming L_o equal to the just-recrystallized grain diameter measured during the recrystallization studies. The values of K at each temperature were logarithmically averaged for each lot and are tabulated in table VI and plotted in figure 5.

As seen in figure 5, the grain growth rates vary considerably among the five lots. Lots B and C exhibited the highest rates at all temperatures while lots D and E exhibited the lowest. Also, the rates for all five lots, showed an approximately linear Arrhenius relation below 3800° F but deviated upward at the higher temperatures.

A comparison of the curves in figure 5 with analytical data for the various lots (table I) suggests a correlation between grain growth behavior and purity. With the exception of lot A, the grain growth rates tend to decrease with increasing impurity content. Minor metallic impurities have been shown to retard grain growth markedly in lead (ref. 27) and tin (ref. 28). No correlation could be found in the present data to show that any one impurity was responsible for the retardation in grain growth in lots D and E.

It is suggested that the low growth rates in lot E, at least, were due to the presence of grain-boundary precipitates. Figure 6 shows evidences of discontinuous grain growth found in lot E after annealing at 4200° F for 1 hour. It has been shown previously (ref. 29) that discontinuous grain growth is caused by partial dissolution or coalescence of grain-boundary precipitates, which retard grain-boundary migration at the lower temperatures. This phenomenon is believed responsible for the sharp increases in K observed above 3800° F.

It is useful here to compare the data given previously with comparable values for commercial powder-metallurgy tungsten. In reference 30, grain sizes were measured for five lots of commercial sheet after tensile and creep testing at temperatures above 3600° F. Four of the five lots were relatively fine grained (4×10^{-3} cm) and did not show any substantial grain growth below approximately 4000° F. This behavior is attributed to a greater density of boundary precipitates in those materials than observed in the present arc-melted materials.

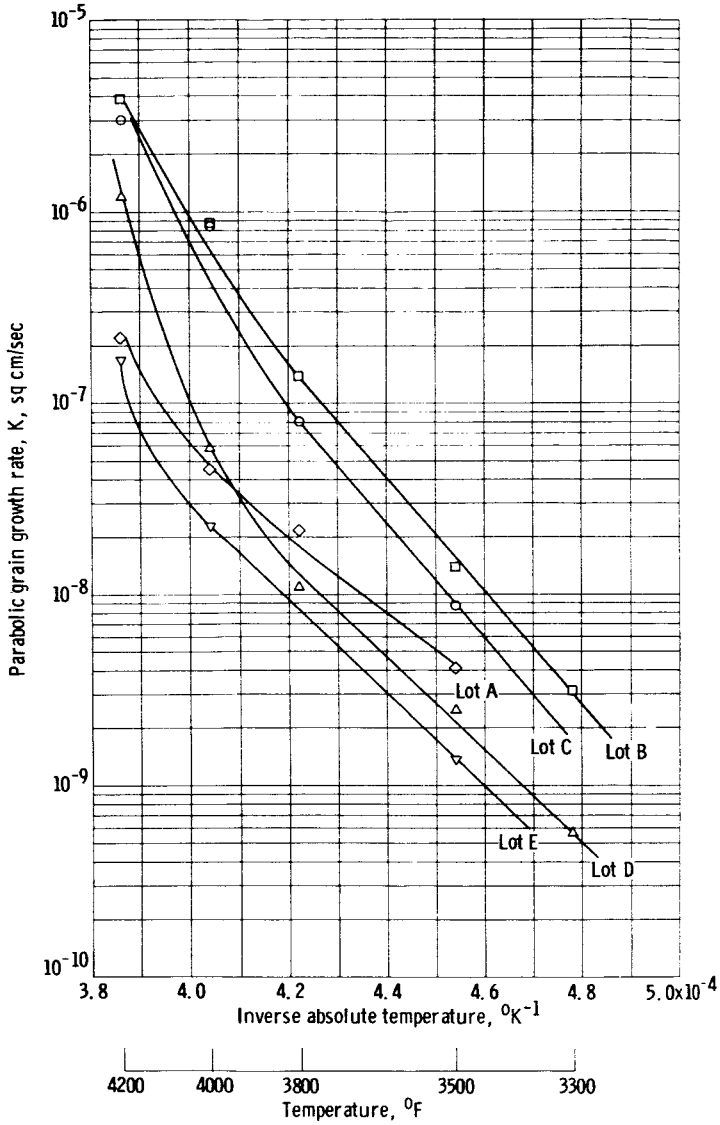

Figure 5. - Temperature dependence of grain growth rates of arc-melted tungsten.

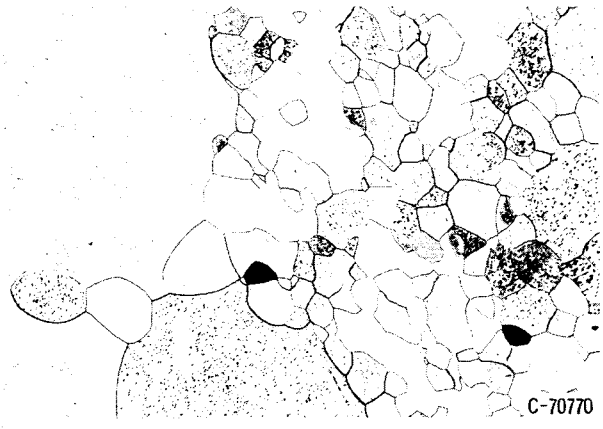

Figure 6. - Lot E, annealed for 1 hour at 4200° F, showing discontinuous grain growth. X100. (Reduced 20 percent in printing.)

Ductile-Brittle Tensile Transition Behavior

Tensile properties of lots A to D were studied at 300° to 750° F in two conditions, stress-relief annealed for 1 hour at 1800° F and recrystallized by a 1-hour anneal at 2900° or 3000° F. Data from these studies are given in table VII. Figure 7 shows a plot of the percent reduction in area against test temperature for the stress-relief-annealed materials, while figure 8 is a similar plot for the recrystallized material. Lack of material precluded a more complete evaluation of these properties.

The stress-relief-annealed materials exhibited a more gradual decrease in ductility with decreasing test temperature than did the fully recrystallized material. The transition temperature (arbitrarily defined as the temperature for 40 percent reduction in area, which reduction is one-half of the maximum of 80 percent expected above the ductile-brittle transition temperature) was lowest for lot D (360±25° F) and highest for lots C (520±25° F) and A (530±50° F).

The transition temperature in this condition followed the usual correlation with the degree of prior warm work. Lot D, with the lowest transition temperature, had 83.6 percent warm reduction, while lot A, with a much higher transition temperature, had only 64.5 percent warm reduction after extrusion. Cold- or warm-working affects the transition temperature through its effect on subgrain size. Finer subgrain sizes or fiber widths have been

TABLE VII. - TENSILE PROPERTIES OF ARC-MELTED TUNGSTEN AT 300° TO 750° F

Annealing condition		Test temperature, °F	0.2-Percent offset yield strength, psi	Ultimate tensile strength, UTS, psi	Elongation, percent	Reduction in area, percent	Transition temperature, °F	Average grain diameter, L, cm
Temperature, °F	Time, t, hr							
Lot A (64.5-percent reduction after extrusion)								
1800	1	450	94,400	107,700	0	4.7	520	---
		550	74,700	85,400	19.0	47.3	---	---
3000	1	625	[a]26,100-22,300	54,000	48.6	46.7	<625	2.26×10^{-2}
		710	[a]20,600-19,700	51,100	52.0	57.5	---	2.26×10^{-2}
Lot B (83.6-percent reduction after extrusion)								
1800	1/4	355	92,400	114,200	14.8	31.0	430	---
		440	86,100	107,000	21.6	41.0	---	---
		495	86,400	97,300	31.2	65.2	---	---
3000	1	490	[a]36,600-31,000	62,800	40.1	29.8	510	1.05×10^{-2}
		570	[a]26,700-23,600	58,800	61.3	65.3	---	---
Lot C (78.2-percent reduction after extrusion)								
1800	1	450	103,500	118,900	23.3	28.5	520	---
		530	87,000	101,000	12.0	41.3	---	---
		650	84,100	93,900	26.8	67.2	---	---
3000	1	750	19,100	54,800	55.0	69.4	<750	9.01×10^{-3}
Lot D (83.6-percent reduction after extrusion)								
1800	1	300	124,500	139,400	14.0	24.5	355	---
		410	99,500	114,900	24.4	53.8	---	---
		510	113,800	123,800	19.0	68.2	---	---
2900	1	520	---	[b]54,400	0	0	>700	---
		700	---	[b]47,300	0	0	---	---

[a]Two values denote upper and lower yield points.
[b]Brittle fracture stress.

shown to result in lower transition temperatures in tungsten (ref. 31).

Although it was not possible to document the ductile-brittle transition behavior of the recrystallized materials fully, it is evident that the transition temperatures were higher than those for the recovery-annealed materials, as expected. Lot B had a transition temperature of 510±50° F, while that for lot A was less than 625° F. The transition temperature greater than 700° F for lot D was somewhat surprising in view of its low transition temperature in the recovery-annealed condition and its finer grain size compared with lots B and C.

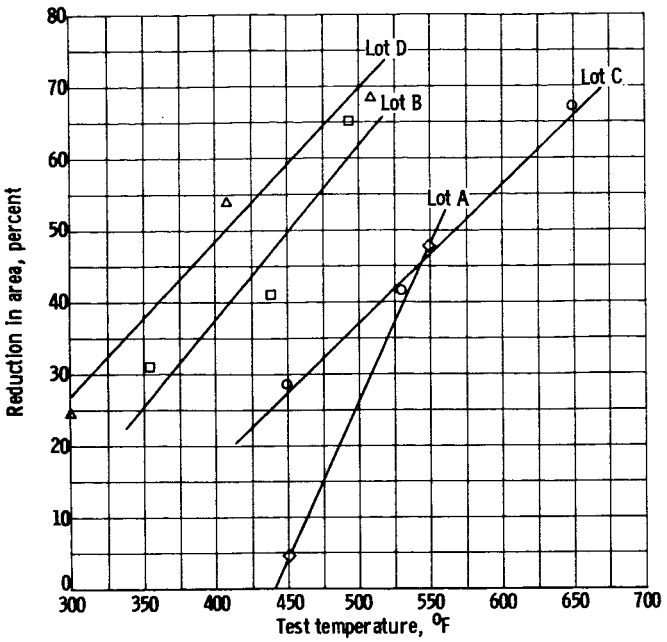

Figure 7. - Ductile-brittle tensile transition behavior of arc-melted tungsten after annealing at 1800° F.

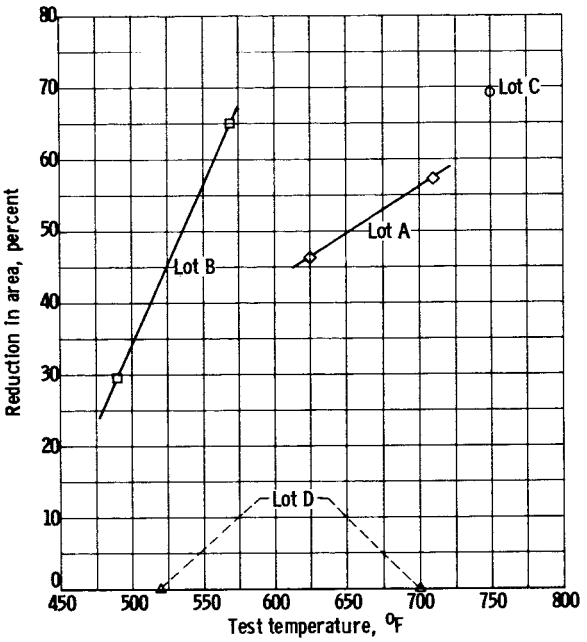

Figure 8. - Ductile-brittle tensile transition behavior of arc-melted tungsten after recrystallization annealing.

Discontinuous yielding, as evidenced by a yield point drop, was observed in all the fully recrystallized materials. Figure 9 shows initial portions of the stress-strain curves for specimens from lots A to C. Lots A and B showed distinct upper and lower yield points, while lot C showed only a Luder's plateau at the lower yield stress. Discontinuous yielding has been observed previously in recrystallized powder-metallurgy tungsten containing 30 parts per million of carbon (ref. 7) and also in commercial powder-metallurgy tungsten after annealing below 2430° F (ref. 25). The present observations cannot be related directly to either of the previous observations, since discontinuous yielding was found here in materials annealed at 2900° or 3000° F and containing only 4 to 9 parts per million of carbon. It appears possible, however, that the processing differences between arc-melted and powder-metallurgy tungsten could affect the distribution of interstitial impurities, so that a given amount of interstitial might be more effective in promoting discontinuous yielding in arc-melted tungsten than in powder-metallurgy tungsten.

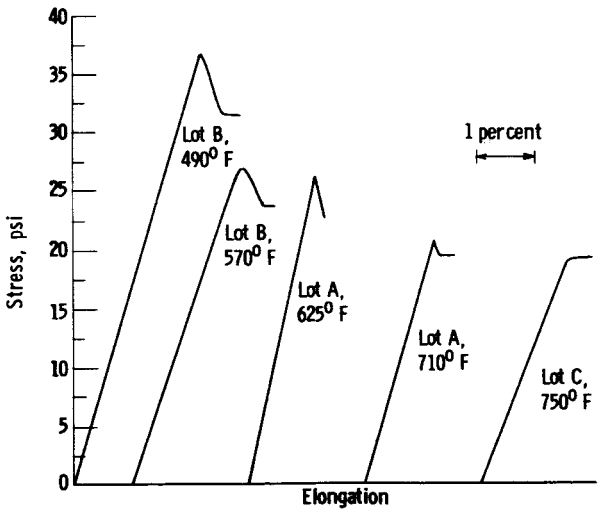

Figure 9. - Types of yielding observed in recrystallized arc-melted tungsten at 490° to 750° F.

Ductile-Brittle Bend Transition Behavior

Bend transition temperatures were determined on sheet rolled from lots B and D after annealing for 1 hour at 1800° to 4200° F. The ductile-brittle transition temperature was defined as the median between the highest temperature at which the material was brittle and the lowest temperature at which it was ductile. These data are presented in table VIII along with the metallographically determined percentage recrystallization and the average grain diameter for each annealing condition. Figure 10 is a plot of the bend transition temperature against the 1-hour annealing temperature for each lot.

TABLE VIII. - DUCTILE-BRITTLE BEND TRANSITION TEMPERATURE OF ARC-MELTED TUNGSTEN SHEET AS-ROLLED AND AFTER ANNEALING FOR 1 HOUR AT 1800° TO 4200° F

Annealing temperature, °F	Ductile-brittle transition temperature, °F	Estimated percent recrystallized	Average grain diameter, L, cm
Lot B			
As-rolled	218	0	----
1800	263	0	----
2000	253	0	----
2200	256	0	----
2300	375	23	----
2400	400	60	----
2500	588	95	----
2600	655	100	1.8×10^{-3}
3000	638	100	5.02×10^{-3}
3400	685	100	1.08×10^{-2}
3700	613	100	2.74×10^{-2}
4000	706	100	[a]$\sim7\times10^{-2}$
Lot D			
As-rolled	212	0	----
2200	275	0	----
3000	595	100	4.04×10^{-3}
3500	675	100	5.55×10^{-3}
4000	668	100	[a]$\sim7\times10^{-2}$
4200	680	100	4.56×10^{-2}

[a]Grain size approximates sheet thickness.

The transition temperature in the as-rolled condition was approximately the same for lots B and D (218° and 212° F, respectively). These are significantly lower than the respective tensile transition temperatures of 440° and 355° F for similar material in the stress-relieved condition. Recovery annealing of lot B and 1800° F increased the transition temperature by about 50° F. Annealing at slightly higher temperatures did not significantly alter this value until the onset of primary recrystallization above 2200° F. After full recrystallization, the transition temperatures remained essentially independent of annealing temperature and of grain size for both lots B and D.

In comparison, the bend transition temperature of worked (92 percent warm reduction) powder-metallurgy sheet is about 212° F (ref. 1). Figure 10 is a comparison of the ductile-brittle transition behavior of this powder-metallurgy sheet compared with lots B and D (83.6 percent warm reduction after extrusion) from the present work. A minimum in the ductile-brittle transition was observed for the powder-metallurgy sheet, while no such minimum was shown in the present work. Annealing above the temperature for the onset of recrystallization resulted in a sharper increase in the ductile-brittle transition for the powder-metallurgy material than for the arc-melted material.

The effects of annealing temperature on the bend transition temperature outlined previously can be compared with those effects on the tensile transi-

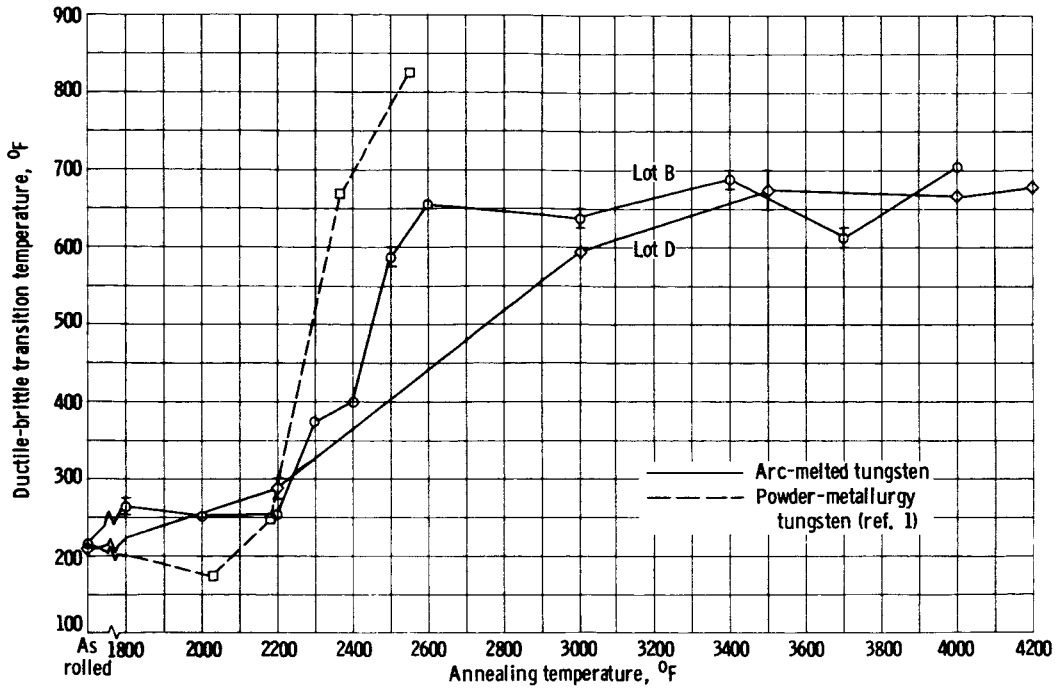

Figure 10. - Ductile-brittle bend transition behavior of arc-melted and powder-metallurgy tungsten annealed for 1 hour. (Upper and lower levels of scatter bands indicate highest temperature at which material was brittle and lowest temperature at which material was ductile, resp.)

tions of powder-metallurgy wire. References 31 and 32 have shown that annealing in the recovery range increases the transition temperatures, presumably because of an increase in the fiber widths observed metallographically. Fiber widths measured on sheet from lot B, annealed at 1800°, 2000°, and 2200° F, ranged from 1.71 to 2.12×10^{-4} centimeter. The small increases in transition temperature on annealing in this temperature range compared with those for the as-rolled materials may be related to small increases in fiber width.

High-Temperature Tensile Properties

High-temperature tensile data were obtained on material from lots B to E in the worked condition and after various annealing treatments. These data are presented in table IX. A plot of the ultimate tensile strength against temperature is shown in figure 11.

Considerable variation in strength properties is observed not only among the four lots studied but also as a function of structure; however, when grain size (measured in the specimen shoulder after testing) is considered, the properties of annealed materials correlate well without regard to lot. A plot of yield and ultimate strength against average grain diameter, shown in figure 12, reveals that the strengths decrease with increasing grain size. The grain-size dependencies, which appear unaffected by temperature over the range from 2500° to 3500° F, may be expressed as

$$YS = AL^{-0.25} \tag{7}$$

TABLE IX. - TENSILE PROPERTIES OF ARC-MELTED TUNGSTEN AT 2500° TO 4140° F

Test temperature, °F	Annealing condition		0.2-Percent offset yield strength, psi	Ultimate tensile strength, UTS, psi	Elongation, percent	Reduction in area, percent	Average grain diameter, L, cm	Strain-hardening coefficient, χ, psi^2
	Temperature, °F	Time, t, hr						
Lot B								
2500	As swaged		31,200	34,000	23.2	95.9	(a)	-----
	3000	1	9,180	23,800	57.4	>98	4.5×10^{-3}	22×10^{8}
3000	1800	1/4	5,700	15,460	61.5	90.5	5.8×10^{-3}	12×10^{8}
	2800	1	4,700	[b]14,500	70.9	93.7	5.6×10^{-3}	12×10^{8}
3500	1800	1/4	4,500	10,230	75.4	91.4	6.7×10^{-3}	5.0×10^{8}
	2800	1	3,830	10,300	76.0	92.5	6.4×10^{-3}	5.5×10^{8}
	4200	4	2,220	7,750	62.9	>95	64×10^{-3}	3.3×10^{8}
4140	1800	1/4	1,500	4,300	73.1	>98	[c]25×10^{-3}	1.3×10^{8}
	2800	1	1,400	4,700	62.6	>98	25×10^{-3}	1.7×10^{8}
Lot C								
2500	As extruded		14,280	25,350	30	90.5	(a)	-------
	As swaged		24,400	36,000	20.3	95.0	(a)	-------
	3600	1	6,420	18,500	57.7	>95	43×10^{-3}	12×10^{8}
3000	As extruded		8,620	16,910	47.8	61.7	(a)	------
	As swaged		18,720	25,100	17.7	83.6	(a)	------
	3600	1	3,940	11,920	38.4	>95	(c)	6.4×10^{8}
3500	As swaged		4,150	10,270	78.9	87.6	9.3×10^{-3}	-------
	3600	1	2,880	8,030	69.2	>95	39×10^{-3}	3.0×10^{8}
	3800	1	2,760	7,880	56.3	>95	46×10^{-3}	3.0×10^{8}
	4000	1	2,690	7,430	61.2	>95	96×10^{-3}	2.5×10^{8}
	4100	1	2,220	7,760	59.1	>95	93×10^{-3}	3.4×10^{8}
	4200	4	2,360	7,500	61.4	>95	108×10^{-3}	3.1×10^{8}

[a]Fully or partly worked microstructure.
[b]Tested at 0.002/0.02 min^{-1}, all other samples tested at 0.005/0.05 min^{-1}.
[c]Grain size estimated from measurements on similar samples.

TABLE IX. - Concluded. TENSILE PROPERTIES OF ARC-MELTED TUNGSTEN AT 2500° TO 4140° F

Test temperature, °F	Annealing condition		0.2-Percent offset yield strength, psi	Ultimate tensile strength, UTS, psi	Elongation, percent	Reduction in area, percent	Average grain diameter, L, cm	Strain-hardening coefficient, χ, psi^2
	Temperature, °F	Time, t, hr						
Lot D								
3000	As swaged		10,200	15,800	49.8	88.9	(a)	-----
	2900	1	17,900	23,400	41.2	98.8	(a)	-----
Lot E								
2500	As swaged		34,700	48,000	16.2	94.3	(a)	-----
	3600	1	10,140	24,450	61.0	94.6	5.2×10^{-3}	21×10^{8}
3000	As swaged		7,650	16,200	74.5	94.0	3.5×10^{-3}	-----
	3600	1	5,430	15,770	80.2	94.8	4.9×10^{-3}	11×10^{8}
3500	As swaged		4,140	10,570	77.2	95.6	4.3×10^{-3}	5.4×10^{8}
	3600	1	4,090	10,240	76.4	95.3	5.3×10^{-3}	4.4×10^{8}
Commercial powder-metallurgy tungsten (ref. 14)[b]								
2500	As received		-----	47,100	25	91	(a, c)	-----
3000	As received		-----	24,400	37	78	(a, c)	-----
3500	As received		-----	10,600	23	36	[c] 3×10^{-3}	-----
4075	As received		-----	6,490	19	25	[c] 3×10^{-3}	-----

[a] Fully or partly worked microstructure.

[b] Tested at 0.002/0.02 min^{-1}, all other samples tested at 0.005/0.05 min^{-1}.

[c] Grain size estimated from measurements on similar samples.

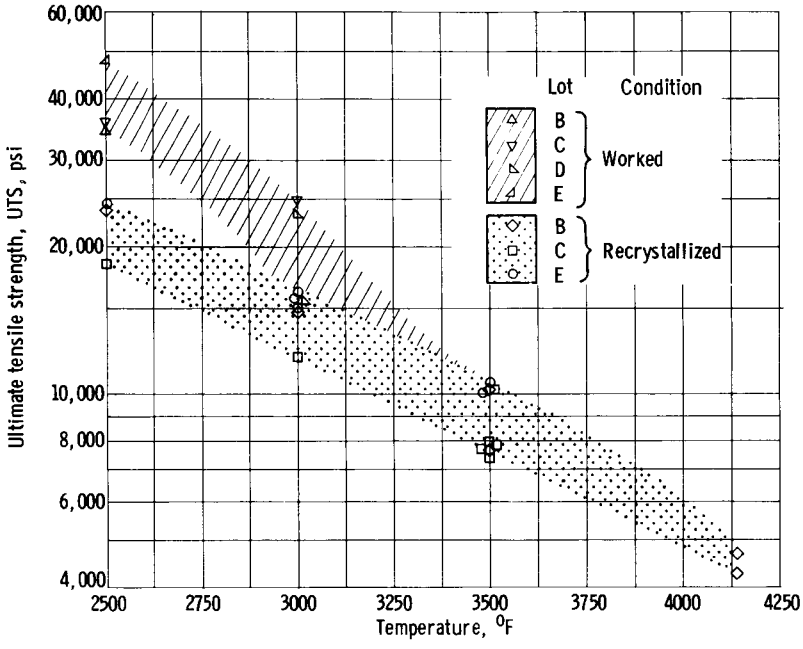

Figure 11. - Effect of temperature on ultimate tensile strength of worked and recrystallized arc-melted tungsten at 2500° to 4140° F.

$$UTS = A'L^{-0.12} \quad (8)$$

where

YS yield strength, psi

UTS ultimate tensile strength, psi

A,A' proportionality factors

L average grain diameter, cm

Thus, decreasing the grain size from 10^{-1} centimeter, typical for arc-melted tungsten annealed above 4000° F, to 5×10^{-3} centimeter, typical for just-recrystallized arc-melted or powder-metallurgy tungsten, increases the yield strength by 80 percent and the ultimate strength by 40 percent. It is also pertinent to note that the less pure materials, such as lot E, had finer grain sizes and hence were stronger than the purer materials, such as lot C. Purity appears to affect the high-temperature strength indirectly, since impurities tend to restrict grain growth and cause a fine-grained structure, which in turn increases the tensile strength.

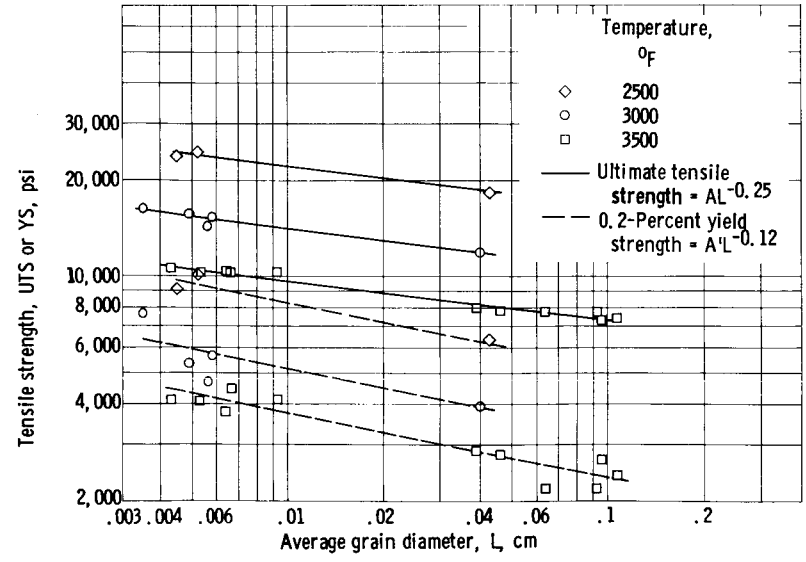

Figure 12. - Effect of grain size on yield and ultimate tensile strengths of arc-melted tungsten at 2500° to 3500° F.

True-stress - true-strain curves were constructed from tensile data for the recrystallized materials by assuming the specimen elongation to be equal to the crosshead motion. These flow curves exhibited the expected parabolic behavior after the initial elastic strain, reflecting the decrease in strain-hardening capacity with increasing plastic strain (refs. 33 and 34). Representative normal and parabolic plots of flow curves are shown in figures 13 and 14.

Strain-hardening co-

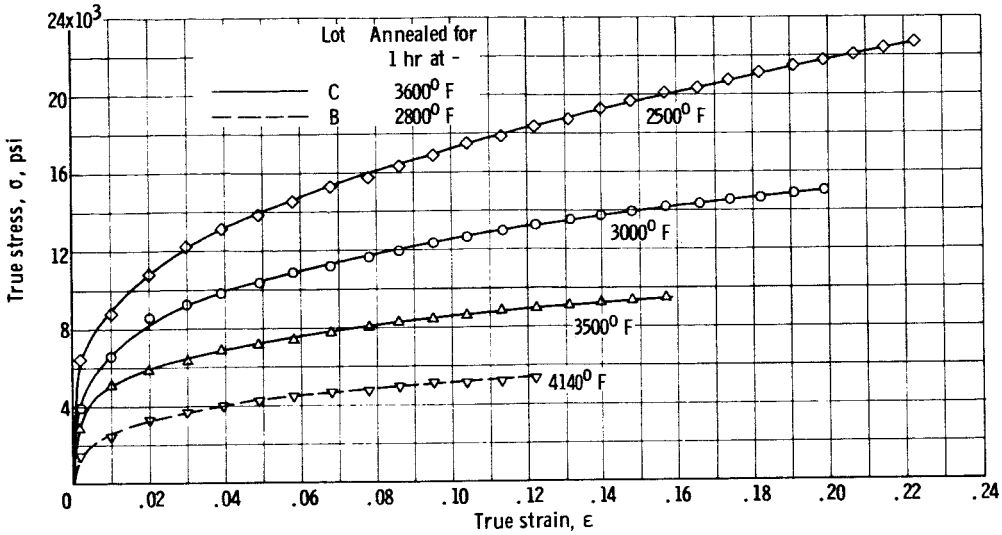

Figure 13. - Effect of temperature on tensile flow curves of arc-melted tungsten at 2500° to 4140° F.

efficients were determined from the relation

$$\chi = \frac{(\sigma - YS)^2}{\epsilon} \tag{9}$$

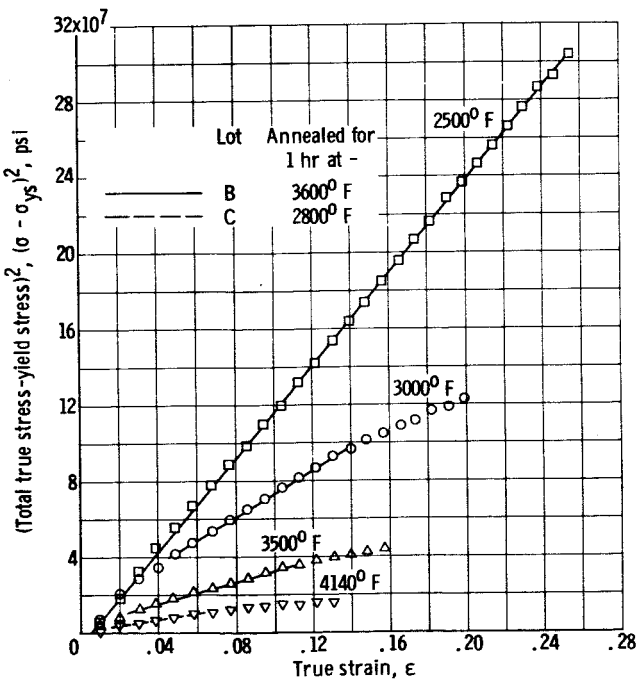

Figure 14. - Parabolic plot of tensile flow curves for arc-melted tungsten at 2500° to 4140° F.

where

χ strain-hardening coefficient, psi^2

σ true stress, psi

YS yield stress, psi

ϵ true plastic strain

These coefficients are included in table IX. As illustrated in figure 14, the experimental data at 2500° F gave a good fit when plotted parabolically, but at higher temperatures, reasonable fits were obtained only at low strains. The deviation at higher strains is attributed to grain-boundary tearing and sliding, which invalidate the assumptions of constant volume and uniform deformation upon which the true-stress - true-strain calculations are based.

The strain-hardening coefficients were also observed to decrease with in-

creasing grain size, as illustrated in figure 15. The grain size dependency varied only slightly if at all with temperature and could be expressed by

$$\chi = BL^{-0.20} \qquad (10)$$

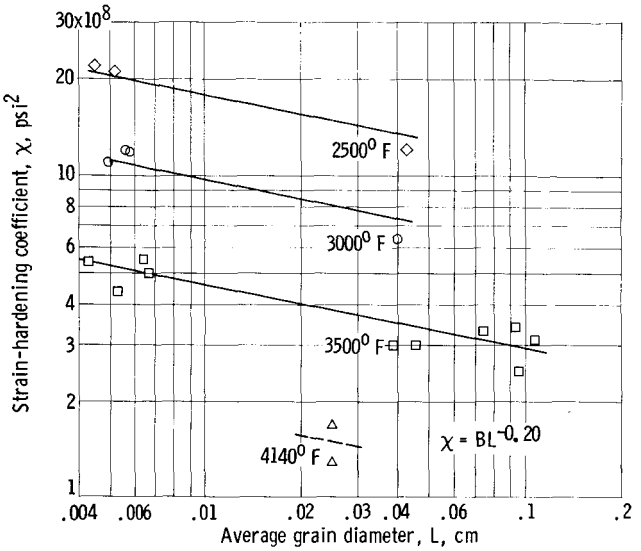

Figure 15. - Effect of grain size on strain-hardening coefficient of arc-melted tungsten at 2500° to 4140° F.

Variations in strength and strain-hardening coefficients with grain size have been observed previously (refs. 35 and 36), although a complete picture of the mechanism has not yet emerged. In reference 36, it has been suggested that the increased strength with decreasing grain size results from the increased complexity of slip within the individual grains. During deformation of a polycrystalline material, the individual grains are partly constrained by their neighbors, so that slip on a given plane can proceed only to the extent that the neighboring grains can deform to accommodate the changing grain shape. As the limit of deformation in a given direction is approached, the resolved stresses within the grain increase, and slip begins on other planes more favorably oriented with respect to the neighboring grains. Decreasing grain size reduces the total strain that can be accommodated on the most favorably oriented slip planes, and the stress increases more rapidly with total strain in order to activate slip on less favorably oriented planes, giving rise to the observed increasing strength and strain-hardening rate with decreasing grain size.

In comparison with arc-melted material, the strength of powder-metallurgy tungsten (ref. 14) included in table IX, is equivalent or slightly higher when compared on the basis of equal grain sizes. At 3500° F the powder-metallurgy tungsten is as strong as fine-grained (5×10^{-3} cm) arc-melted tungsten, while at 4100° F the powder-metallurgy material is about 40 percent stronger than the fine-grained arc-melted materials. The major difference between the two materials, however, lies in their high-temperature ductilities. While arc-melted tungsten is relatively ductile at all temperatures above its ductile-brittle transition temperature, powder-metallurgy tungsten exhibits low ductility in the temperature range of 2500° to 4000° (ref. 14). This low ductility may be associated with grain-boundary pinning by impurities, which restricts the extent to which grains may deform to accommodate the intragranular slip (ref. 37).

High-Temperature Creep-Rupture Properties

Constant-load creep studies were conducted at 3000° and 3500° F on worked and annealed materials from lots A and E, with results as presented in table X. Step-load creep studies were also conducted at 3000°, 3500°, and 4000° F on

TABLE X. - CONSTANT CREEP-RUPTURE DATA FOR ARC-MELTED TUNGSTEN AT 3000° AND 3500° F

Annealing condition		Stress, psi	Transient creep rate, $sec^{-1/3}$	Steady creep rate, sec^{-1}	Rupture time, t_r, min	Total elongation, percent	Reduction in area, percent	Average grain diameter, L, cm
Temperature, °F	Time, t, hr							
Lot E Test temperature, 3000° F								
As swaged		7,240	---	1.79×10^{-6}	2673.1	81.2	85.4	7.3×10^{-3}
		11,210	---	[a]3.62-9.8	429.2	62.0	93.0	5.3
4100	1	4,760	1.50×10^{-3}	0.507×10^{-6}	6541.8	44.2	35.9	27×10^{-3}
		6,010	4.26	3.37	1353.6	63.8	52.6	9.6
		7,390	5.36	13.5	257.7	40.6	>98	19.5
Lot A Test temperature, 3500° F								
4100	1	2,300	0.961×10^{-3}	0.343×10^{-6}	[b]6100	----	----	92×10^{-3}
		3,020	---	1.43	1486.0	30.8	>98	187
		5,150	---	72.1	35.9	32.3	>98	182
4200	1	1,980	0.690×10^{-3}	0.131×10^{-6}	[c]6785.0	----	---	---
		2,470	---	.742	[d]9168.5	22.0	14.0	146×10^{-3}
		3,040	---	1.43	1191.3	44.1	15.1	70
		5,040	---	20.3	189.2	22.4	31.8	137
Lot E								
As swaged		2,980	---	0.637×10^{-6}	4790.4	35.8	32.7	5.6×10^{-3}
		5,130	---	6.14	714.6	61.5	61.7	5.5
4100	1	2,400	0.864×10^{-3}	0.215×10^{-6}	[b]>3800	>9.0	>4.6	12.7×10^{-3}
		3,580	---	2.32	1207.2	31.7	66.2	11.5

[a]Rate increased from 3.62×10^{-6} to 9.8×10^{-6} sec^{-1} after 100 min.

[b]Estimated rupture time.

[c]Load increased to 2470 psi.

[d]Total life including 6785 min at 1980 psi.

[e]Test discontinued.

material from lots D, F, and G. Data on the step-load tests are presented in table XI.

Representative creep curves, shown in figures 16 and 17, indicate that the creep behavior of tungsten in this temperature range may be represented by periods of transient or primary creep, steady or secondary creep, and tertiary creep. During transient creep, strain hardening occurs more rapidly than does thermal recovery, causing the instantaneous creep rate to diminish with time. As the creep rate decreases, a balance is achieved between the rates of strain hardening and recovery, giving a constant creep rate. Tertiary creep is generally associated with necking of the specimen and/or the formation of internal voids at the grain boundaries.

TABLE XI. - STEP-LOAD CREEP DATA FOR ARC-MELTED TUNGSTEN AT 3000° TO 4000° F

Lot	Annealing condition		Stress, lb/sq in.	Steady creep rate, sec^{-1}	Total elongation, percent	Total reduction in area, percent	Average grain diameter, L, cm
	Temperature, °F	Time, t, hr					
Test temperature, 3000° F							
F	4000	1	7,980	26.3×10^{-6}	-----	-----	-----
			8,970	40	-----	-----	-----
			10,080	84	-----	-----	-----
			10,980	210	[a]36.5	[a]20.4	32.2×10^{-3}
G	4200	1	7,480	43.4×10^{-6}	-----	-----	-----
			8,470	81.3	-----	-----	-----
			9,500	200	[a]37.8	[a]17.2	114×10^{-3}
Test temperature, 3500° F							
D	3600	1	5,020	15.7×10^{-6}	-----	-----	-----
			5,480	19.7	-----	-----	-----
			5,990	30	-----	-----	-----
			6,540	52.6	-----	-----	-----
			6,970	96.6	[a]23.4	[a]15.6	7.21×10^{-3}
	3800	1	4,490	10.7×10^{-6}	-----	-----	-----
			5,030	15.3	-----	-----	-----
			5,490	21.4	-----	-----	-----
			5,970	30.7	-----	-----	-----
			6,490	55	-----	-----	-----
			6,990	110	[a]22.6	[a]12.5	10.45×10^{-3}
F	4000	1	4,720	19.5×10^{-6}	-----	-----	-----
			5,530	36.2	-----	-----	-----
			6,220	68.8	-----	-----	-----
			6,940	171	72.9	>98	38.3×10^{-3}
			5,030	25	-----	-----	-----
			5,530	35	-----	-----	-----
			6,000	60	-----	-----	-----
			6,480	115	69.0	>98	32.6×10^{-3}
Test temperature, 4000° F							
F	4000	1	2,600	18.3×10^{-6}	-----	-----	-----
			2,890	26.7	-----	-----	-----
			3,180	41.2	-----	-----	-----
			3,490	73.4	[a]18.4	[a]9.8	29.7×10^{-3}
G	4200	1	2,310	21.7×10^{-6}	-----	-----	-----
			2,590	30	-----	-----	-----
			2,880	50.3	-----	-----	-----
			3,180	93.3	[a]26.1	[a]16.3	97.6×10^{-3}

[a]Test discontinued.

The steady creep rate in the temperature range where thermal recovery is possible may be represented by a relation of the following form (ref. 38):

$$\dot{e} = k_s \sigma^a L^b e^{-Q/RT} \qquad (11)$$

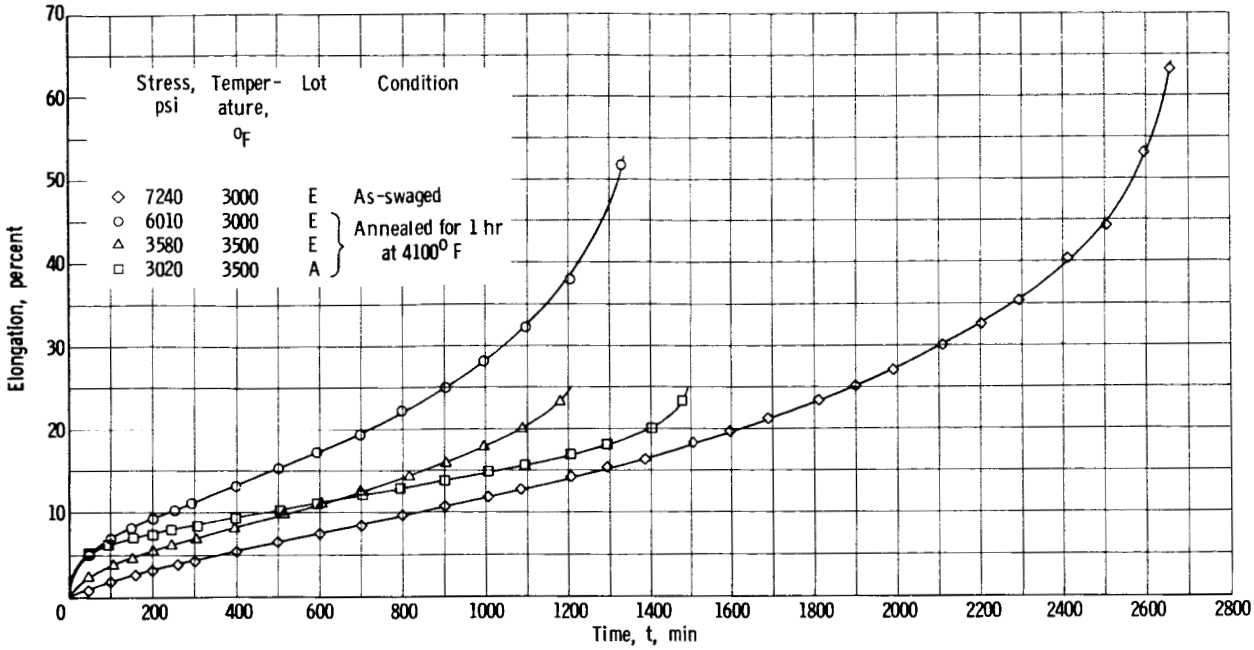

Figure 16. - Representative constant-load-creep curves for arc-melted tungsten at 3000° and 3500° F.

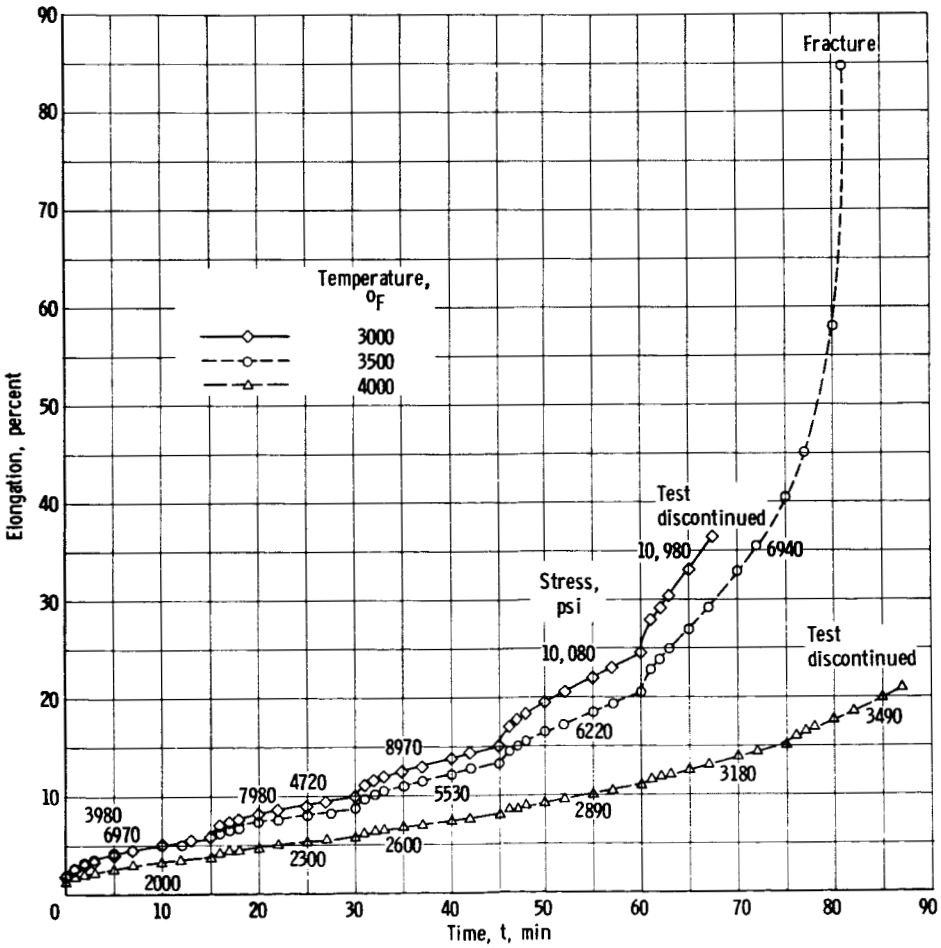

Figure 17. - Representative step-load creep curves for arc-melted tungsten at 3000°, 3500°, and 4000° F. Lot F annealed for 1 hour at 4000° F.

where

$\dot{e}$ steady creep rate, sec^{-1}

k constant

s engineering stress, psi

a exponential stress dependency

L average grain diameter, cm

b exponential grain size factor

Q activation energy for creep, cal/g-mole

R gas constant, 1.987 cal/g-mole

T temperature, ^{o}K

Values for the exponential stress dependency a commonly range from 4 to 6, while Q at high temperatures is usually similar to the activation energy for self-diffusion (refs. 36 and 38).

A plot of the steady creep rates against stress, shown in figure 18, shows

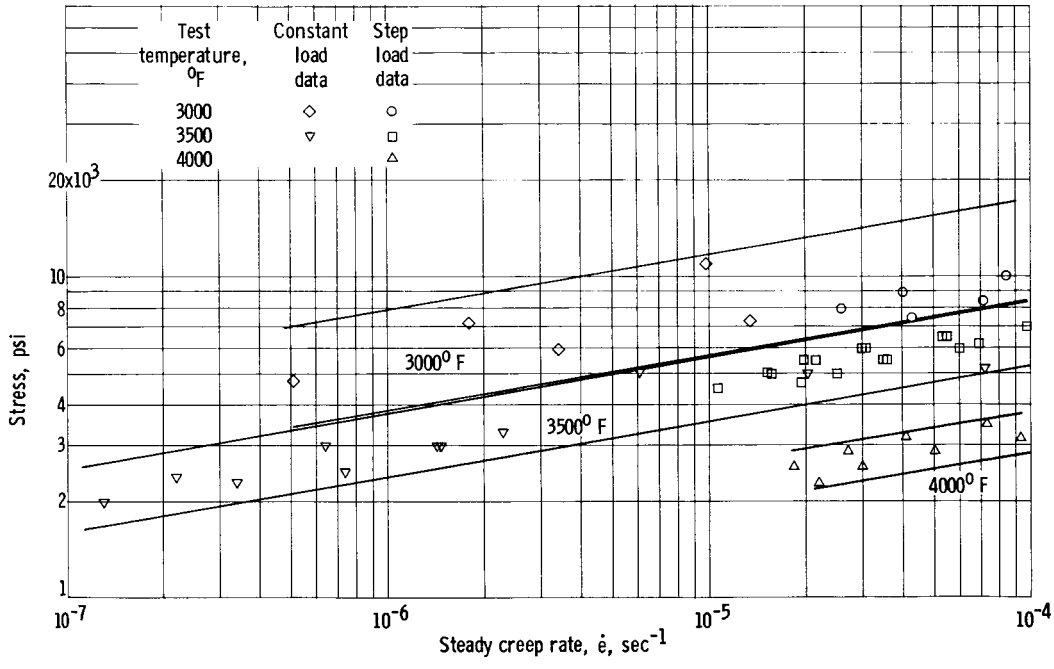

Figure 18. - Steady creep rate against stress for arc-melted tungsten, illustrating range of data obtained.

wide scatter in the data for each temperature. This scatter was considerably reduced by introducing the grain-size factor. A least-squares analysis of the

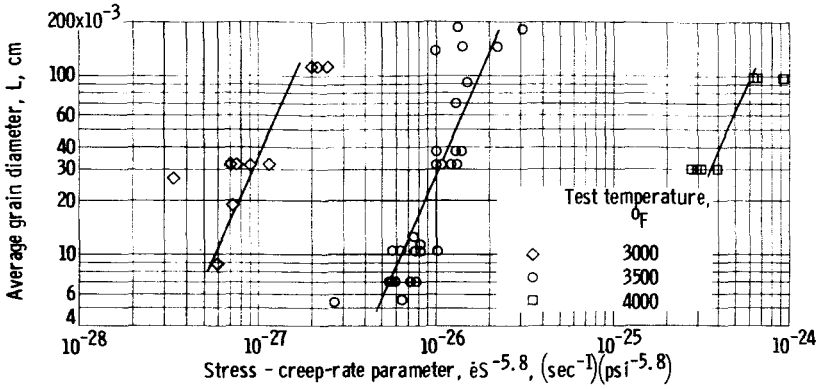

Figure 19. - Effect of grain size on stress - creep-rate parameter for arc-melted tungsten at 3000° to 4000° F.

data gave average values of 5.8 and 0.43 for a, the exponential stress factor, and b, the exponential grain-size factor, respectively. As seen from equation (11) the grain-size dependencies at each temperature can be illustrated by a plot of L against $\dot{e}S^{-a}$, while the stress dependency can be illustrated by plotting S against $\dot{e}L^{-b}$. The grain-size dependency is shown in figure 19, while the structure - creep-rate parameter against stress is shown in figure 20. The exponential stress dependency a decreases slightly with increasing temperature, ranging from 6.5 at

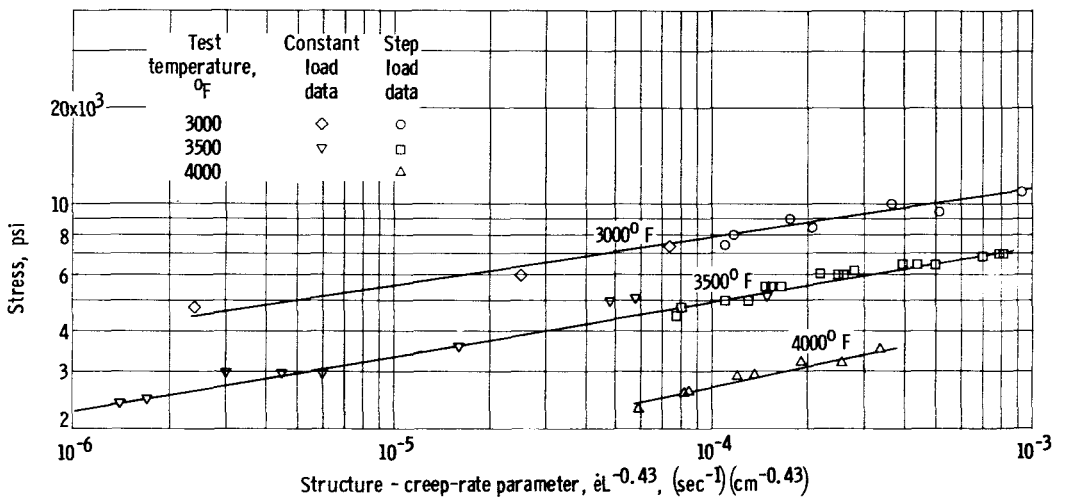

Figure 20. - Structure - creep-rate parameter against stress for arc-melted tungsten showing good fit obtained when creep rates are compensated for grain size.

3000° F to 4.6 at 4000° F (where only step-load-rate data were obtained). This factor appears as the slopes of the lines in figure 20.

The average value of 5.8 for a in the current study is close to the values of 6.3 for powder metallurgy tungsten at 4082° to 5072° F (ref. 39) and 5 at 4800° F (ref. 30).

The grain-size factor b of 0.43 is less than the value of 2 proposed in a recent review (ref. 38) and observed in copper (ref. 40) and in powder-metallurgy tungsten (ref. 30). The increase in creep rate with increasing grain size in the present study, however, is in qualitative agreement with these and other recent observations (refs. 41 to 43). In contrast, studies on

aluminum (ref. 36) and other metals (refs. 44 and 45) have shown the opposite effect of grain size, the coarse-grained materials being more creep resistant than the fine-grained materials. The reasons for these conflicting observations on the effects of grain size have not yet been satisfactorily explained.

The temperature dependency of the creep constant k is shown in figure 21. It is seen that the slope decreases with decreasing temperature, corresponding to a change in the activation energy from about 140 kilocalories per gram-mole between 3500° and 4000° F to about 74 kilocalories per gram-mole between 3000° and 3500° F. In previous studies on aluminum (ref. 36), a decrease in activation energy from 35 kilocalories per gram-mole to 28 kilocalories per gram-mole with decreasing temperature at about 0.5 Tm was attributed to a change in mechanism from dislocation climb at the higher temperature to cross slip at the lower temperature. Since the activation energy of 140 kilocalories per gram-mole is fairly close to that for self-diffusion, 153 kilocalories per gram-mole (ref. 22), the creep mechanism at 3500° to 4000° F may be dislocation climb. The decrease in temperature dependency at 3000° to 3500° F probably represents a transition in the rate controlling reactor from dislocation climb to cross slip.

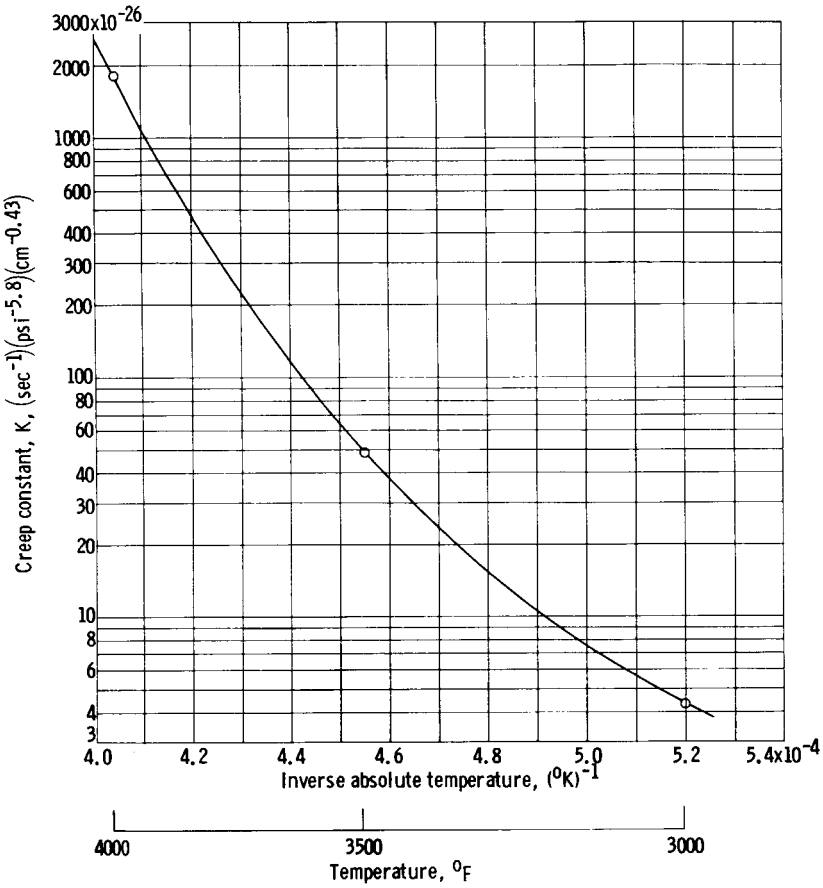

Figure 21. - Temperature dependence of creep constant for arc-melted tungsten at 3000° to 4000° F.

The transient or primary creep flow was also studied at 3000° and 3500° F in order to characterize more completely the high-temperature creep behavior of tungsten and to determine the relation between the transient and steady flow rates. The initial portions of the constant-load creep curves were correlated according to the familiar Andrade relation

$$e = \beta t^{1/3} \tag{12}$$

where

e engineering strain

β transient creep rate, $sec^{-1/3}$

t time, sec

Representative plots are shown in figure 22, and rate data are included in table X.

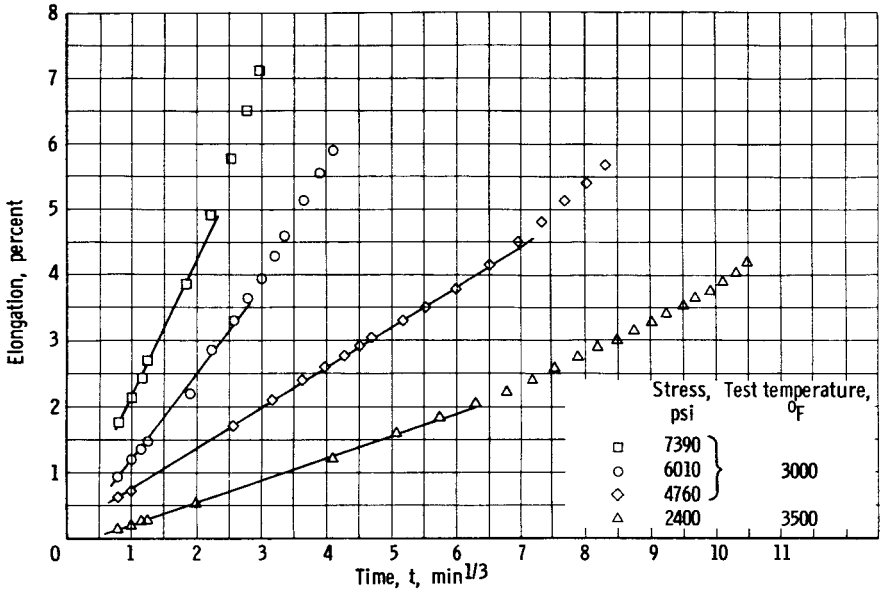

Figure 22. - Cubic plot of transient creep of arc-melted tungsten at 3000° and 3500° F. Lot E; annealed for 1 hour at 4100° F.

In figure 23, the transient creep rates are compared with the steady creep rates. It is seen that, for annealed materials, the rates at both 3000° and 3500° F may be correlated by a parabolic relation

$$\dot{e} = 0.3\ \beta^2 \tag{13}$$

This type of relation has previously been observed in copper (ref. 40) and columbium (ref. 46), while data for lead (ref. 41) showed similar ratios between $\dot{e}$ and β but tended to exhibit a cubic rather than a parabolic relation. For columbium the proportionality constant was about 0.1, compared with 0.3 observed in the present study.

Cubic creep was not observed for specimens that were initially in the swaged condition. Apparently, the swaged materials were undergoing structural changes (recrystallization and/or grain growth), which significantly affected

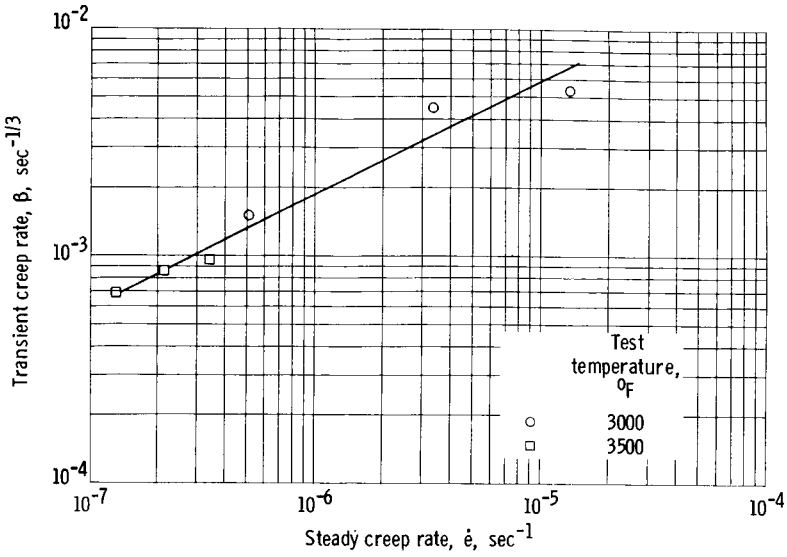

Figure 23. - Relation between transient and steady creep rates for annealed arc-melted tungsten at 3000° and 3500° F.

the transient creep behavior.

The relation between steady creep rate and rupture life is shown in figure 24. This relation may be expressed as

$$t_r = \left(\frac{c}{\dot{e}}\right)^m \tag{14}$$

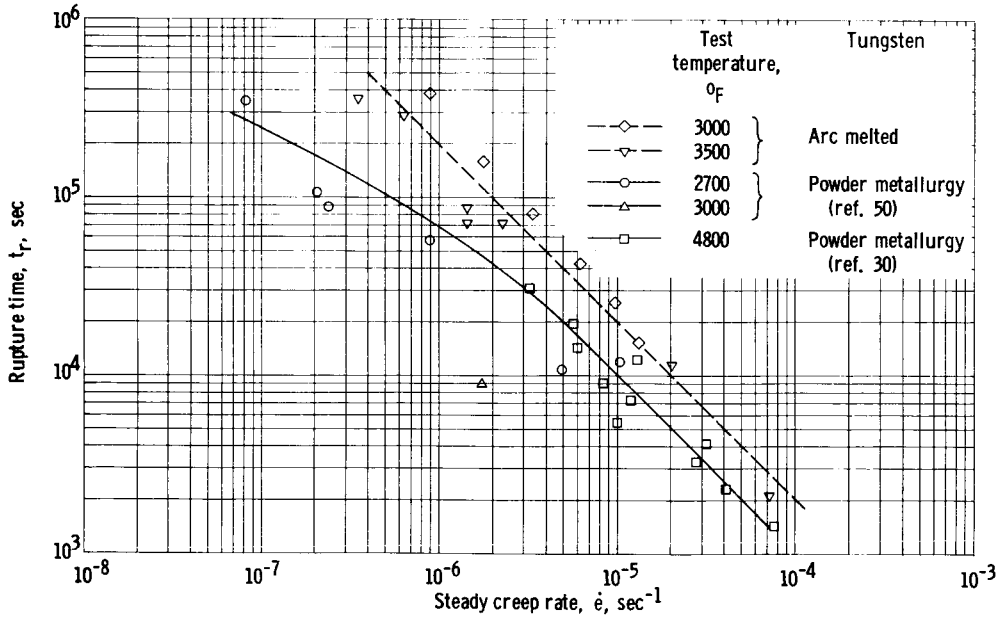

Figure 24. - Relation between steady creep rate and rupture time for arc-melted and powder-metallurgy tungsten.

where $m = 1.0$ for the present data and $c = 0.2$. Data for arc-melted molybdenum (ref. 47) also show a linear relation ($m = 1.0$) with $c = 0.35$, while for copper (ref. 40), $m = 1$ also, but c is smaller, 0.06. By comparison, in reference 48, it was found that m ranges from 0.77 to 0.93 for a variety of materials including aluminum, titanium, steels, and superalloys. Values for m of less than unity probably indicate that extraneous reactions (aging, strain-induced precipitation hardening, etc.) are affecting the creep behavior.

It is of practical interest to compare the data on rupture life against steady creep rate for arc-melted tungsten with the limited data available on powder-metallurgy tungsten. This comparison affords an indication of the creep ductility of various materials. In figure 24, rupture life and steady creep rates for both arc-melted and powder-metallurgy tungsten (refs. 30 and 49) are plotted. It is seen that for a given creep rate. the rupture life of powder-metallurgy tungsten is about one-half that of arc-melted tungsten. The difference in behavior between powder-metallurgy and arc-melted tungsten is further shown by rupture data at 2700° and 3000° F (fig. 25). Arc-melted fine-

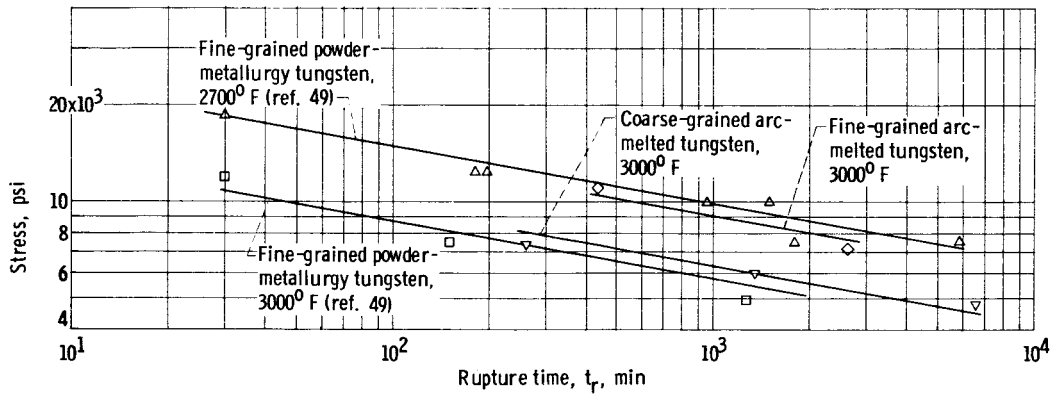

Figure 25. - Rupture time against stress for arc-melted and powder-metallurgy tungsten at 2700° and 3000° F.

grained tungsten, which would be expected to exhibit a creep rate similar to that of powder-metallurgy tungsten (because of expected similar grain sizes) had by far the longer rupture life. Large-grained arc-melted tungsten exhibited about the same life as powder-metallurgy tungsten. This difference is thought to result from the presence of fine particles in the powder-metallurgy tungsten that severely restrict grain-boundary mobility during deformation and thus reduce the ductility.

From the limited data available, it appears that, for similar temperature and stress levels, unalloyed powder-metallurgy tungsten may exhibit lower creep rates than unalloyed arc-melted tungsten because of the relatively stable fine grain size of the former. This advantage is somewhat offset by the longer rupture life of arc-melted materials for a given creep rate. Arc-melted tungsten alloys can be expected to compare even more favorably with similar powder-metallurgy tungsten alloys, since they will also possess finer, more stable grain sizes than unalloyed arc-melted tungsten.

The internal and external structural features of specimens deformed at

various flow rates (both creep and tension) were studied in order to gain further insight into the mechanisms of flow and fracture. Figures 26 to 31 show

(a) Surface view showing slip lines and grain-boundry sliding. X15.

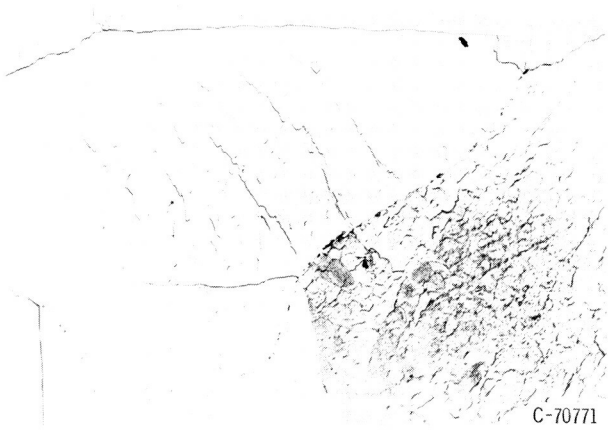

(b) Internal view showing polyganization and microvoids (stress axis horizontal). X100.

Figure 26. - Coarse-grained tensile specimen. Lot C; annealed for 4 hours at 4200° F; tested at 3500° F; strain rate, 8.4×10^{-4} sec^{-1}. (Reduced 20 percent in printing.)

(a) Surface view showing slip lines and grain-boundary separation. X15.

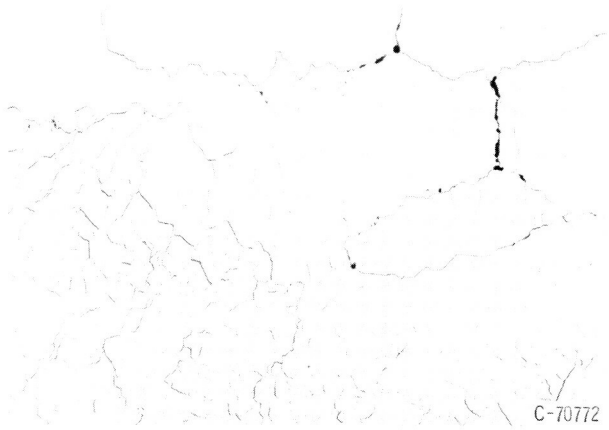

(b) Internal view showing polyganization and small grain-boundary voids (stress axis horizontal). X100.

Figure 27. - Coarse-grained creep specimen. Lot A; annealed for 4 hours at 4200° F; tested under high stress (5040 psi) at 3500° F; steady creep rate, 2.03×10^{-5} sec^{-1}. (Reduced 20 percent in printing.)

representative external macrostructures and internal microstructures of both coarse- and fine-grained specimens deformed to fracture at flow rates of 8.4×10^{-4} $second^{-1}$ (0.05 min^{-1} tensile test) to 6.3×10^{-7} $second^{-1}$ (slow creep).

Significant observations from this series of specimens may be summarized as follows:

(1) At high flow rates (figs. 26 and 29), the surfaces exhibit numerous coarse slip markings and considerable grain deformation. Recent studies of slip in tungsten at ambient (ref. 50) and elevated temperatures (ref. 51)

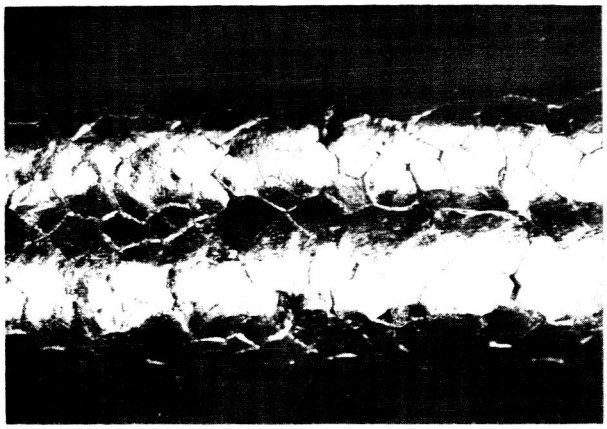

(a) Surface view showing grain-boundary separation. X15.

(b) Internal view showing transverse grain-boundary voids and polyganization (stress axis horizontal). X100.

Figure 28. - Coarse-grained creep specimen. Lot A; annealed for 4 hours at 4200° F; tested under low stress (1980 to 2470 psi) at 3500° F; steady creep rate, 1.31 to 7.42X10^{-7} sec^{-1}. (Reduced 20 percent in printing.)

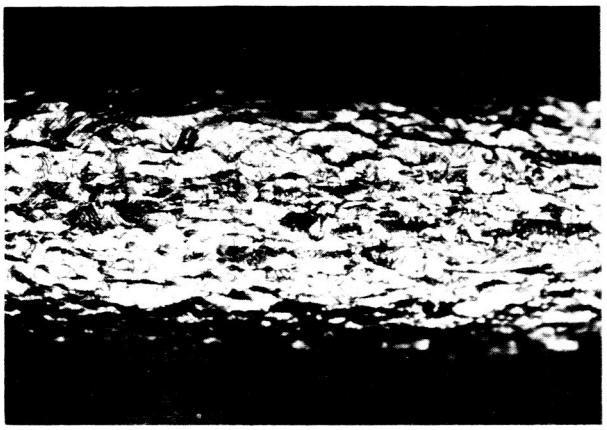

(a) Surface view showing slip lines. X15.

(b) Internal view showing polyganization and longitudinal tearing (stress axis horizontal). X100.

Figure 29. - Fine-grained tensile specimen. Lot E; annealed for 1 hour at 3600° F; tested at 3500° F; strain rate 8.4X10^{-4} sec^{-1}. (Reduced 20 percent in printing.)

suggest that these markings represent normal or cross-slip traces of (112) planes slipping in the ⟨111⟩ direction. Deformation at low flow rates (figs. 28 and 31) appears to have been accommodated primarily by boundary sliding and separation.

(2) Micrographs show that high flow rates (figs. 26 and 29) promote polygonization and serrated grain boundaries (indicative of deformation by coarse slip), while low flow rates (figs. 28 and 31) promote less polygonization and only slightly deformed grain boundaries.

(3) At all strain rates, voids were found at the grain boundaries and appeared to have formed initially at triple boundary junctions. At high flow rates (fig. 29), voids were elongated parallel to the tension axis; at intermediate flow rates (fig. 30), voids were irregular; at low flow rates, voids were larger and were oriented transverse to the tension axis.

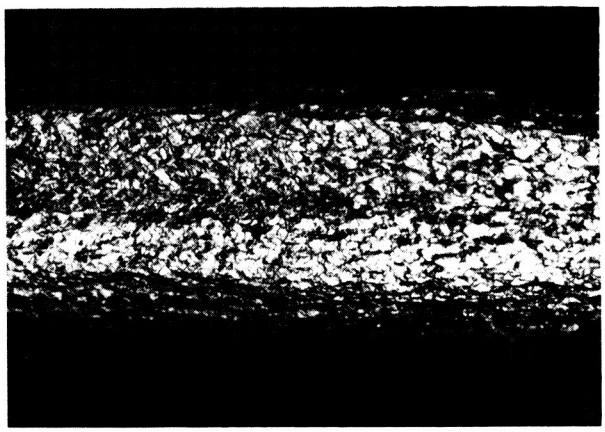

(a) Surface view showing grain-boundary sliding. X15.

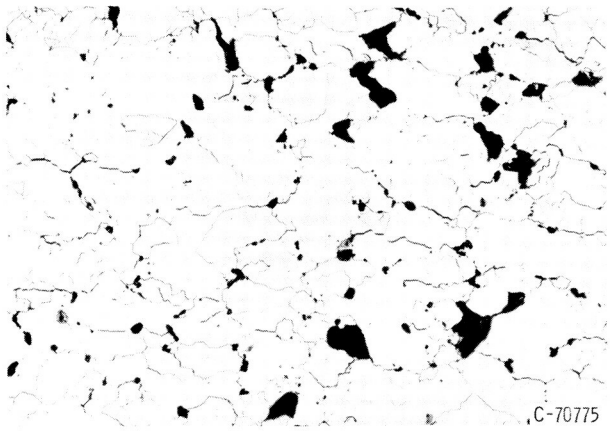

(b) Internal view showing grain-boundary tearing (stress axis horizontal). X100.

Figure 30. - Fine-grained creep specimen. Lot E; as swaged; tested under high stress (5130 psi) at 3500° F; steady creep rate, 6.14×10^{-6} sec^{-1}. (Reduced 20 percent in printing.)

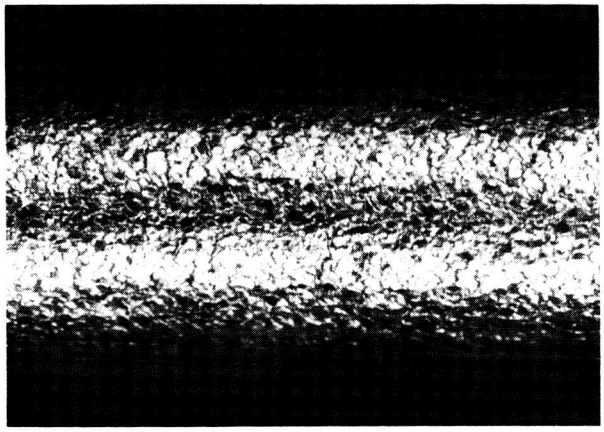

(a) Surface view showing grain-boundary tearing. X15.

(b) Internal view showing grain-boundary voids transverse to stress direction (stress axis horizontal). X100.

Figure 31. - Fine-grained creep specimen. Lot E; as swaged; tested under low stress (2980 psi) at 3500° F; steady creep rate, 6.37×10^{-7} sec^{-1}. (Reduced 20 percent in printing.)

(4) Void density was mugh higher in the fine-grained materials than in the coarse-grained materials.

These observations are consistent with recent views on the processes of high-temperature deformation and fracture as summarized in references 37 and 52. According to these views, jogs at the grain boundary, produced by intragranular slip, and triple points serve as barriers to grain-boundary sliding during high-temperature deformation at moderately high flow rates. As flow proceeds, the stress concentration at these barriers increases until relieved by boundary sliding, grain deformation, or tearing. In the latter case, voids are formed, which normally exhibit little growth and become mechanically elongated parallel to the tensile axis as deformation proceeds. At low flow rates, thermal recovery eliminates slip traces, which produce grain-boundary jogs, but triple points remain as barriers to grain sliding. Voids formed at these triple points grow by vacancy condensation, which becomes important as the time

available for diffusion of vacancies increases. Surface tension effects cause the growing voids to elongate transverse to the tension axis, as illustrated in figures 28(b) and 31(b).

Grain-size effects on void formation are particularly evident in the present work. The increase in void density with decreasing grain size is attributed to increased complexity of intragranular slip caused by the shorter available slip distance, which produces a larger number of grain-boundary jogs, and to the larger number of triple points.

CONCLUSIONS

A study of the effects of purity and structure on recrystallization, grain growth, low temperature ductility, tensile, and creep properties of arc-melted tungsten yielded the following conclusions:

1. The recrystallization behavior of arc-melted tungsten follows the usual pattern, increasing prior strains and longer annealing times decreasing the temperatures for full recrystallization. The strain-induced boundary migration rates, calculated from recrystallization data, varied among the five lots studied, but appeared to decrease with increasing detectable metallic impurity content. The observed activation energy approximates that expected for grain-boundary self-diffusion.

2. The grain growth behavior also appeared to be related to impurity content. The growth rates tended to decrease with increasing detectable metallic impurities.

3. Arc-melted tungsten exhibits ductile-brittle transition temperatures in tension and in bending which are similar to those reported for powder-metallurgy tungsten. The tensile transition temperatures for stress-relief-annealed materials showed the usual tendency to decrease with increasing prior work.

4. The yield and ultimate tensile strengths and the parabolic strain-hardening coefficients of arc-melted tungsten at 2500° to 4140° F decrease significantly with increasing grain size. For example, the ultimate strength, which is proportional to the -0.12 power of grain size, is increased by 40 percent on decreasing the grain size from 0.1 to 0.005 centimeter. The strength of arc-melted tungsten is similar to that reported for powder-metallurgy tungsten when compared at similar grain sizes, although the former exhibits better high-temperature ductility.

5. The creep behavior of arc-melted tungsten at 3000° to 4000° F was also significantly affected by grain size, the finer-grained material being more creep resistant. The initial transient flow behavior followed the expected cubic relation. The cubic rates for annealed materials are related to the subsequent linear flow rates. The temperature dependency for linear creep corresponds to an activation energy of approximately 140 kilocalories per gram-mole

between 3500° and 4000° F but apparently decreases between 3000° and 3500° F.

Lewis Research Center
National Aeronautics and Space Administration
Cleveland, Ohio, July 23, 1964

APPENDIX - SPECTROGRAPHIC ANALYSES OF ARC-MELTED TUNGSTEN

Conventional chemical and emission spectrographic analyses on four starting electrodes and on fabricated rods from lots A to E are given in table XII. A comparison between the starting electrode and the fabricated rod analyses for lots B, D, and E does not appear warranted since the analyses were conducted at different laboratories. The analyses for lot C starting electrode and fabricated rod, however, were conducted at the same laboratories. Comparison of these two analyses reveals only minor detectable changes in composition as a result of melting and fabrication. Oxygen, nitrogen, nickel, and sulfur are seen to be lower in the fabricated rod, while carbon, copper, iron, and molybdenum are higher. The small increases in carbon and copper levels could result from contamination by the carbonaceous diffusion pump oil and the copper crucible during melting, but the increases in iron and molybdenum are unexplainable, if real. It may be fairly concluded that melting and fabrication produce only minor detectable compositional changes in tungsten if high-purity electrode material is used.

TABLE XII. - CHEMICAL AND EMISSION SPECTROGRAPHIC ANALYSES OF TUNGSTEN STARTING ELECTRODES AND FABRICATED RODS

Element	Impurity, ppm[a]						
	Starting electrodes		Fabricated rods				
	Lot						
	B,D,E[b]	C	A	B	C	D	E
Oxygen	6±5	11	3	2	6	5	3
Nitrogen	<6	15	13	9	8	9	12
Carbon	10	8	6	4	9	6	5
Hydrogen	<6	<1	<1	<1	<1	<1	<1
Aluminum	10	10	2	3	10	10	20
Calcium	10	--	<10	<10	<10	<10	<10
Chromium	10	<5	<5	<5	<5	<5	7
Copper	10	<1	2	1	1	1	5
Iron	10	10	5	20	20	20	60
Magnesium	10	--	--	--	--	--	--
Manganese	10	<1	<1	<1	<1	<1	<1
Molybdenum	10	<10	15	15	15	15	15
Nickel	10	8	2	2	2	2	10
Potassium	--	<10	<10	<10	<10	10	<10
Silicon	10	10	10	5	10	10	15
Sodium	--	<10	<10	10	<10	20	10
Sulfur	--	18	<10	<10	<10	<10	<10
Tin	10	<5	<5	<5	<5	<5	<5
Total detectable metallics	110	56	36	56	58	88	142

[a]Analyses conducted as follows:
Oxygen and hydrogen - vacuum fusion
Carbon - combustion
Nitrogen - Kjeldahl
Sulfur - combustion
Metallics - emission spectrography

[b]Analysis from supplier.

Mass spectrographic analyses on fabricated rods from lots A to E are presented in table XIII. These analyses were obtained on a recently developed double-focusing unit capable of high resolution. The impurity levels observed by mass spectrography are generally lower than those observed by emission spectrography for the same elements.

For several elements, the two spectrographic techniques give different results. For example, emission spectrography indicated lot B to have the lowest silicon content of the five lots studied, while mass spectrography showed the same lot to have the highest silicon content. The two methods are in agreement, however, as to the relative purities of the five lots. Both methods indicate that the total impurity level increases in the order A, B, C, D, E.

TABLE XIII. - MASS SPECTROGRAPHIC ANALYSIS

OF FABRICATED TUNGSTEN RODS

Element	Lot				
	A	B	C	D	E
	Impurity, ppm				
Aluminum	1.0	1.4	6.0	0.1	10.0
Antimony	<.04	<.03	<.01	.05	.3
Arsenic	.008	.05	.01	.05	.008
Boron	<.01	<.01	<.01	4.0	<.01
Calcium	5.0	1.0	4.0	1.0	5.0
Chromium	1.0	.1	.1	.1	.1
Cobalt	.03	.3	:01	.2	.025
Copper	.2	.4	.45	.4	.2
Iron	3.0	2.5	3.0	13.0	15.0
Lithium	<.01	<.01	<.01	.05	<.01
Magnesium	<.05	<.05	<.05	.1	.1
Manganese	<.01	.05	<.01	.05	<.01
Molybdenum	4.0	6.0	5.0	9.5	6.0
Nickel	.3	.4	.3	.2	1.1
Phosphorus	.2	.025	.2	.15	.2
Potassium	1.0	<1.0	1.0	<1.0	2.0
Silicon	5.0	11.0	5.0	4.0	9.0
Sodium	<.05	<.05	<.05	11.0	<.05
Sulfur	.25	.3	.2	1.0	.2
Tin	<.01	<.01	<.01	<.01	.01
Vanadium	<.05	.1	<.05	.2	<.05
Zinc	.03	<.01	.04	.01	.03
Total detectable metallics	21.0	24.0	25.0	45.0	49.0

REFERENCES

1. Ogden, H. R.: Department of Defense Refractory Metals Sheet-Rolling Program. DMIC-176, Status Rep. 2, Defense Metals Info. Center, Oct. 15, 1962.

2. Foyle, Fred A.: Arc-Melted Tungsten and Tungsten Alloys. High Temperature Materials, pt. II. AIME Metall. Soc. Conf., Vol. 18, G. M. Ault, W. F. Barclay and H. P. Munger, eds., Interscience Pub., 1963, pp. 109-124.

3. Harmon, E. L.: Properties of Tungsten and Tungsten Base Alloys. Investigation of the Properties of Tungsten and Its Alloys, Sec. III. TR 60-144, WADD, May 1960.

4. Allen, Banjamin C., Maykuth, Daniel J., and Jaffee, Robert I.: The Effects of Impurities on the Properties of Tungsten. TR 60-6, Air Force Special Weapons Center, Dec. 15, 1959.

5. Atkinson, Russell H., et al.: Physical Metallurgy of Tungsten and Tungsten Base Alloys. TR 60-37, WADD, May 1960.

6. Stern, Milton: Fabrication and Properties of Tungsten and Tungsten Alloy Single Crystals. Final Rep. by Staff of Linde and Haynes Stellite Co., Div. Union Carbide Corp., Mar. 31, 1962.

7. Stephens, J. R.: Effects of Interstitial Impurities on the Ductility of Tungsten. Paper Presented at AIME meeting, New York (N.Y.), Oct. 29-Nov. 1, 1962.

8. Koo, R. C.: Effect of Purity on the Tensile Properties of Tungsten Single Crystals from -196° C to 29° C. Acta Met., vol. 11, no. 9, Sept. 1963, pp. 1083-1095.

9. Witzke, Walter R., Sutherland, Earl C., and Watson, Gordon K.: Preliminary Investigation of Melting, Extruding, and Mechanical Properties of Electron-Beam-Melted Tungsten. NASA TN D-1707, 1963.

10. Clark, J. W.: Flow and Fracture of Tungsten and Its Alloys: Wrought, Recrystallized, and Welded Conditions. TDR-63-420, Aeronautical System Div., Apr. 1963.

11. Noesen, S. J.: The Removal of Gaseous Impurities by Vacuum Arc Melting. Vacuum Symposium Trans., Am. Vacuum Soc., Pergamon Press, 1958, pp. 150-156.

12. Anon.: Standard Methods for Estimating the Average Grain Size of Metals. ASTM Standards, pt. 3. ASTM, 1961.

13. Stephens, Joseph R.: Effect of Surface Condition on the Ductile-to-Brittle Transition Temperature of Tungsten. NASA TN D-676, 1961.

14. Sikora, Paul F., and Hall, Robert W.: High-Temperature Tensile Properties of Wrought Sintered Tungsten. NASA TN D-79, 1959.

15. Burke, J. E., and Turbbull, D.: Recrystallization and Grain Growth. Progress in Metal Phys., Vol. 3, Pergamon Press, 1952, pp. 220-292.

16. Gatti, A., and Fullman, R. L.: A Study of the Recrystallization Kinetics and Tensile Properties of an Internally Oxidized Solid-Solution Silver-Aluminum Alloy. Trans. AIME, vol. 215, no. 5, Oct. 1959, pp. 762-769.

17. Weissmann, S.: Growth Processes in Recrystallization of Aluminum. Trans. ASM, vol. 53, 1961, pp. 265-281.

18. Weissmann, S., Imura, T., and Hosokawa, N.: Recrystallization and Grain Growth of Aluminum. Proc. of Symposium on Recovery and Recrystallization of Metals. L. Himmel, ed., Intersci. Pub., 1963, p. 241.

19. Pugh, J. W.: On the Recovery and Recrystallization of Tungsten. Plansee Proc. 1958, Pergamon Press, 1959, pp. 97-107.

20. Feltham, P., and Copley, G. J.: Grain-Growth in α-brasses. Acta Met., vol. 6, no. 8, Aug. 1958, pp. 539-542.

21. Cole, D. G., Feltham, P., and Gillam, E.: On the Mechanism of Grain Growth in Metals, with Special Reference to Steel. Proc. Phys. Soc. (London), sec. B, vol. 67, Feb. 1954, pp. 131-137.

22. Andelin, R. L.: Self-Diffusion in Single-Crystal Tungsten and Diffusion of Rhemium Tracer in Single-Crystal Tungsten. Rep. LA-2880, Los Alamos Sci. Lab., Apr. 1963.

23. Gordon, Paul., and Vandemeer, R. A.: The Mechanism of Boundary Migration in Recrystallization. Trans. AIME, vol. 224, no. 5, Oct. 1962, pp. 917-928.

24. Aust, K. T., and Rutter, J. W.: Temperature Dependence of Grain Boundary Migration in High-Purity Lead Containing Small Additions of Tin. Trans. AIME, vol. 215, no. 5, Oct. 1959, pp. 820-831.

25. Koo, R. C.: Recovery in Cold-Worked Tungsten. Jour. Less-Common Metals, vol. 3, no. 5, Oct. 1961, pp. 412-428.

26. Feltham, P.: Grain Growth in Metals. Acta Met., vol. 5, no. 2, Feb. 1957, pp. 97-105.

27. Bolling, G. F., and Winegard, W. C.: Some Effects of Impurities on Grain Growth in Zone-Refined Lead. Acta Met., vol. 6, no. 4, Apr. 1958, p. 283.

28. Holmes, E. L., and Winegard, W. C.: The Effect of Lead and Bismuth on Grain Growth in Zone-Refined Tin. Trans. AIME, vol. 224, no. 5, Oct. 1962, pp. 945-949.

29. Beck, P. A., Holzworth, M. L., and Sperry, P. R.: Effect of a Dispersed Phase on Grain Growth in Al-Mn Alloys. Trans. AIME, vol. 180, 1949, pp. 163-192.

30. Sutherland, E. C., and Klopp, William D.: Observations of Properties of Sintered Wrought Tungsten Sheet at Very High Temperatures. NASA TN D-1310, 1963.

31. Seigle, L. L., and Dickinson, C. D.: Effect of Mechanical and Structural Variables on the Ductile-Brittle Transition in Refractory Metals. Refractory Metals and Alloys, pt. II, M. Semchysen and I. Perlmutter, eds., Interscience Pub., Inc., 1963, p. 65.

32. Lement, B. S., et al.: Substructure and Mechanical Properties of Refractory Metals. TR-61-181, pt. II, WADD, Oct. 1962.

33. Clarebrough, L. M., and Hargreaves, M. E.: Work Hardening of Metals. Prog. in Metal Phys., Vol. 8, Pergamon Press, 1959, pp. 1-104.

34. Wasilewski, R. J.: On Discontinuous Yield and Plastic Flow in α-Titanium. Trans. ASM, vol. 56, no. 2, June 1963, pp. 221-235.

35. Gensamer, M.: The Effect of Grain Boundaries on Mechanical Properties. Relation of Properties to Microstructure, ASM, Cleveland, 1954, p. 16.

36. McLean, D.: Mechanical Properties of Metals. John Wiley & Sons, Inc., 1962.

37. Grant, N. J.: Intercrystalline Failure at High Temperatures. Fracture, M.I.T. Tech. Press and John Wiley & Sons, Inc., 1959, pp. 562-578.

38. Sherby, O. D.: Factors Affecting the High Temperature Strength of Polycrystalline Solids. Acta Met., vol. 10, no. 2, Feb. 1962, pp. 135-147.

39. Green, W. V.: Short-Time Creep-Rupture Behavior of Tungsten at 2250° to 2800° C. Trans. AIME, vol. 215, no. 6, Dec. 1959, p. 1057.

40. Feltham, P., and Meakin, J. D.: Creep in Face-Centered Cubic Metals with Special Reference to Copper. Acta Met., vol. 7, no. 9, Sept. 1959, pp. 614-627.

41. Feltham, P.: On the Mechanism of High-Temperature Creep in Metals with Special Reference to Polycrystalline Lead. Proc. Phys. Soc. (London), sec. B, vol. 69, Dec. 1956, pp. 1173-1188.

42. Anon.: High Temperature Materials Program Progress. Rep. GEMP-23A, General Electric Co., May 31, 1963.

43. Parker, Earl R.: Modern Concepts of Flow and Fracture. Trans. ASM, vol. 50, 1958, pp. 52-104.

44. Sully, A. H.: Metallic Creep and Creep Resistant Alloys. Intersci. Pub., Inc., 1949.

45. Clark, Claude Lester: High-Temperature Alloys. Pitman Pub. Corp., 1953.

46. Brinson, G., and Argent, B. B.: The Creep of Niobium. Jour. Inst. Metals, vol. 91, no. 9, May 1963, pp. 293-297.

47. Houck, J. A.: Physical and Mechanical Properties of Commercial Molybdenum-Base Alloys. Rep. 140, Defense Metals Info. Center, Nov. 30, 1960.

48. Monkman, F. C., and Grant, N. J.: An Empirical Relationship Between Rupture Life and Minimum Creep Rate in Creep-Rupture Tests. Proc. ASTM, vol. 56, 1956, p. 593.

49. Sell, Heinz G., et al.: Physical Metallurgy of Tungsten and Tungsten Base Alloys. TR-60-37, pt. II, WADD, May 1961.

50. Garlick, R. G., and Probst, H. B.: Investigation of Room-Temperature Slip in Zone-Melted Tungsten Single Crystals. Trans. Metall. Soc. AIME, vol. 230, no. 5, Aug. 1964, pp. 1120-1125.

51. Berlac, I.: On the Deformation of Polycrystalline Tungsten at High Temperatures. Acta Met., vol. II, no. 1, Jan. 1963, pp. 68-70.

52. Gifkins, R. C.: Mechanisms of Intergranular Fracture at Elevated Temperatures. Fracture, M.I.T. Tech. Press and John Wiley & Sons, Inc., 1959, pp. 579-627.